

Inhibition of ATR Reverses a Mitochondrial Respiratory Insufficiency

Megan B. Borrer¹, Milena Girotti¹, Adwitiya Kar¹, Meghan Cain¹, Xiaoli Gao², Vivian L. MacKay³, Brent Herron⁴, Shylesh Bhaskaran¹, Sandra Becerra¹, Nate Novy⁵, Natascia Ventura^{6,7}, Thomas E. Johnson⁴, Brian K. Kennedy^{3,8,9}, Shane L. Rea^{1,5,10*}

¹The Barshop Institute for Longevity and Aging Studies, ²Department of Biochemistry, and ¹⁰Department of Physiology, University of Texas Health Science Center at San Antonio, San Antonio, TX 78229, USA.

³Department of Biochemistry, and ⁵Department of Pathology, University of Washington, Seattle, WA 98195, USA

⁴Institute for Behavioral Genetics & Department of Integrative Physiology, University of Colorado at Boulder, Boulder, CO 80309, USA.

⁶IUF — Leibniz Research Institute for Environmental Medicine, Düsseldorf, Germany.

⁷Institute for Clinical Chemistry and Laboratory Diagnostic, Medical Faculty of the Heinrich Heine University, Düsseldorf, Germany

⁸Buck Institute for Research on Aging, Novato, CA 94945, USA.

⁹Departments of Biochemistry and Physiology, Yong Loo Lin School of Medicine, National University of Singapore, Singapore

*Address correspondence to: Shane Rea, PhD; University of Washington, Department of Pathology, 1959 NE Pacific St., Box 357470, Seattle WA 98195-7470.

ABSTRACT

Diseases that affect the mitochondrial electron transport chain (ETC) often manifest as threshold effect disorders, meaning patients only become symptomatic once a certain level of ETC dysfunction is reached. Multiple processes work to control proximity to the critical ETC threshold and as a consequence there can be significant variability in disease presentation among patients. Identification of such control processes remains an ongoing goal. Checkpoint signaling comprises a collection of alert mechanisms activated in cells in response to nuclear DNA damage. Well-defined hierarchies of proteins are involved in both sensing and signaling DNA damage, with ATM (ataxia telangiectasia mutated) and ATR (ATM and Rad3-related) acting as pivotal signaling kinases. In the nematode *C. elegans*, severe reduction of mitochondrial ETC activity shortens life, as in humans, but mild

32 reduction extends life as a consequence of survival strategies that are invoked under these
33 circumstances. Here we show that removal of ATL-1, the worm ortholog of ATR, unexpectedly lessens
34 the severity of ETC dysfunction, but removal of ATM does not. Multiple genetic and biochemical tests
35 show no evidence for increased mutation or DNA breakage in animals exposed to ETC disruption.
36 Instead, we find that reduced ETC function alters nucleotide ratios within both the ribo- and deoxyribo-
37 nucleotide pools, and causes stalling of RNA polymerase, which is also known to activate
38 ATR. Unexpectedly, *atl-1* mutants confronted with mitochondrial ETC disruption maintain normal levels
39 of oxygen consumption and have an increased abundance of translating ribosomes. This suggests
40 checkpoint signaling by ATL-1 normally dampens cytoplasmic translation. Taken together, our data
41 suggests a model whereby ETC insufficiency in *C. elegans* results in nucleotide imbalances leading to
42 stalling of RNA polymerase, activation of ATL-1, dampening of global translation and magnification of
43 ETC dysfunction. Loss of ATL-1 effectively reverses the severity of ETC disruption so that animals
44 become phenotypically closer to wild type.

45

46 **Short Title:** Reversing a mitochondrial electron transport chain insufficiency

47 **Keywords:** Aging, ageing, checkpoint response, DNA damage response, DDR, MAK-1, MAK-2,
48 MAPKAPs, Mit mutants, polysome profiling, retrograde response.

49

50 **Abbreviations:** **ATM**, ataxia telangiectasia mutated; **ATFS-1**, Activating Transcription Factor
51 associated with Stress; **ATL-1**, ataxia telangiectasia mutated-Like (*C. elegans* ortholog of ATR); **ATR**,
52 ataxia telangiectasia mutated and Rad3-related; **DDR**, DNA damage response; **DHODH**, dihydroorotate
53 dehydrogenase; **DNA pol α** , DNA polymerase alpha; **DNA polA1**, DNA polymerase alpha catalytic
54 subunit; **ETC**, electron transport chain; **mtDNA**, mitochondrial DNA; **MAPKAP**, p38 MAPK-activated
55 protein kinase; **mTOR**, mechanistic target of rapamycin; **PIKK**, phosphoinositide 3-kinase-related

56 kinase; **R-loop**, DNA::RNA hybrid; **RNA pol II**; RNA polymerase II; **TUNEL**, Terminal deoxynucleotidyl
57 transferase dUTP nick end labeling.

58

59 **INTRODUCTION**

60 The essential nature of mitochondria is underscored by the devastating effects of inherited
61 mitochondrial diseases which afflict approximately one in 5000 children and almost always result in
62 pathological shortening of life ¹. Because these organelles play central roles in many cellular
63 processes, including energy production, nucleotide metabolism and apoptotic signaling ^{2, 3, 4}, their
64 progressive, age-dependent reduction in function means almost all of us, at some time in life, will
65 experience the negative consequences of mitochondrial dysfunction ⁵. Indeed a growing number of
66 age-related ailments common to western societies are either associated with, or directly caused by,
67 mitochondrial disruption ^{6,7}.

68 In *Caenorhabditis elegans*, as in humans, mitochondrial dysfunction is threshold dependent.
69 That is, a critical level of electron transport chain (ETC) dysfunction must be reached before pathology
70 is observed ⁸. Nematodes with high levels of mitochondrial dysfunction exhibit shortened lifespan and
71 reduced fitness, while worms with moderate levels of mitochondrial dysfunction display extended
72 lifespan ⁹. This response is evolutionarily conserved from yeast to mammals and understanding the
73 molecular mechanisms regulating lifespan extension in worms in response to mild ETC disruption may
74 provide insight into strategies that could be applied to help keep our own cells above their critical
75 mitochondrial dysfunction threshold.

76 Reduced ETC activity disrupts many downstream cellular processes and as might be expected
77 cells have evolved a variety of sensors and strategies to counter progression toward their critical ETC
78 threshold. Multiple signaling pathways, collectively called retrograde responses, are activated within
79 cells and these in turn control expression of nuclear counter-measures ¹⁰. For example, an increase in
80 the unfolded protein load of the mitochondrial matrix re-directs the transcription factor ATFS-1 from the

81 matrix to the nucleus where it stimulates expression of mitochondrial chaperones¹¹. Other signals such
82 as changes in calcium concentration, activation of mitogen-activated protein kinases (MAPKs), and
83 even knock-on changes in the cytoplasmic unfolded protein load, also result in retrograde response
84 activation^{12, 13, 14}. Counter-measures that are activated by cells include increased mitochondrial
85 biogenesis, elevated mitochondrial DNA (mtDNA) replication, increased mitophagy, activation of
86 alternate pathways of energy production (such as glycolysis), and changes in the abundance and
87 activity of respiratory complexes or their regulatory factors^{8, 15, 16}. The complete network of pathways
88 that detect and respond to mitochondrial stress is, however, far from being fully understood¹⁷.

89 Previously, we described a phenomenon in worms in which loss of CEP-1, a homolog of the
90 human p53 checkpoint protein that recognizes identical DNA sequences and is the only p53 family
91 member present in *C. elegans*¹⁸, right shifted the mitochondrial ETC threshold, effectively allowing
92 animals to cope with a greater degree of mitochondrial ETC disruption and consequently mitigating the
93 lifespan shortening effects of severe mitochondrial dysfunction¹⁹. This response was due to alterations
94 in autophagy and lipid metabolism, both of which are regulated by CEP-1²⁰. In the current study, we
95 examined the role of other checkpoint proteins in modulating the mitochondrial threshold effect of
96 worms since this is still a little-explored area of investigation.

97 Ataxia-telangiectasia mutated (ATM) and 'ATM- and *rad3*-related' (ATR) are two well-studied
98 members of the phosphoinositide 3-kinase-related kinase (PIKK) family of proteins that play essential
99 roles in transducing checkpoint signaling during the DNA damage response (DDR)²¹. In humans, both
100 proteins together directly phosphorylate over 900 sites on some 700 proteins, including p53²². ATM
101 and ATR differ in the lesions to which they are recruited, with ATM being recruited to dsDNA breaks
102 and ATR having a broader specificity underscored by the presence of ssDNA, including recessed
103 dsDNA breaks and stalled replication forks²³. Depending on the level of damage and success of repair,
104 checkpoint activation can lead to pro-survival or pro-apoptotic mechanisms²⁴. Recently, additional
105 functions were ascribed to both ATM and ATR. For ATM, these involve regulation of a variety of
106 processes, including insulin signaling, the pentose phosphate pathway and mitophagy. Also, in yeast,

107 ATM/Tel1p was found to act as a specific sensor of mitochondria-generated ROS^{25, 26, 27, 28, 29}. ATR on
108 the other hand was shown to be important in controlling an outer mitochondrial membrane (OMM)-
109 localized apoptotic signal, autophagy, RNA polymerase activity and chromatin condensation^{30, 31, 32, 33,}
110³⁴. In this study, we uncover a new role for ATR in mitochondrial retrograde response signaling.

111

112 RESULTS

113 Loss of ATL-1/ATR desensitizes worms to mitochondrial ETC stress

114 In *C. elegans*, *atp-3* encodes the ortholog of the human ATP5O/OSCP subunit of the mitochondrial
115 F₁F₀ ATP synthase, while *isp-1* encodes the Rieske Fe-S ortholog of complex III. We have previously
116 reported that wild type worms exposed to increasing amounts of bacterial feeding RNAi targeting either
117 *atp-3* or *isp-1* reach a critical threshold after which the concentration of RNAi causes worms to exhibit a
118 reduction in body size and an extension of lifespan³⁵. For *isp-1* RNAi, life extension follows a
119 monotonic function, while for *atp-3* RNAi, life is first extended then it is pathologically shortened³⁵.
120 These 'mean lifespan versus feeding RNAi dosage' curves were mapped using 12 point datasets and
121 their profiles were robust across multiple rounds of testing³⁵. This differing effect of *atp-3* and *isp-1*
122 feeding RNAi on lifespan reflects the more potent degree of ETC inhibition that is ultimately attained
123 following severe *atp-3* knockdown. Using these well-defined treatment regimes and reagents, we tested
124 whether loss of ATM-1 or ATR checkpoint proteins altered the phenotypic response of worms to
125 mitochondrial ETC disruption (see **Supplemental File S1** for a full description of mutants used in this
126 study and the method used to propagate lethal DDR strains). When mutant *atm-1(gk186)* worms
127 were exposed to *atp-3* or *isp-1* RNAi (1/10th strength and undiluted) animals matured and survived
128 indistinguishably from similarly-treated wild type worms (**Fig. 1A-D**). In contrast, *atl-1(tm853)* mutants
129 were differentially refractory to the effects of knockdown of either RNAi. This effect was most evident in
130 worms treated with 1/10th strength *atp-3* or *isp-1* RNAi, where animals showed obvious resistance to
131 both size reduction (**Fig. 1A, B**) and lifespan extension (**Fig. 1C, D**). (Additional examples are
132 presented later in **Figure 2A-C**). *atp-3* and *isp-1* knockdown did eventually reduce adult size and

133 extend life in the mutant *atl-1(tm853)* background, suggesting the response to ETC disruption in these
134 animals is right-shifted relative to wild type control (see schematic **Fig. 1C, D**). Surprisingly,
135 measurement of *atp-3* and *isp-1* mRNA levels following RNAi treatment revealed that target gene
136 knockdown was as efficacious in *atl-1(tm853)* mutants as it was in wild type worms (**Fig. 1E**), indicating
137 these animals were not deficient for RNAi. Furthermore, we found that *atl-1(tm853)* mutants were also
138 refractory to mitochondrial ETC disruption induced using chemical inhibition (**Supplemental Figure**
139 **S1**). Based on these findings, we conclude that inhibition of the phosphoinositide 3-kinase-related
140 kinase ATL-1 confers resistance to mitochondrial ETC disruption.

141

142 **Figure 1. Loss of ATL-1 desensitizes worms to mitochondrial respiratory chain stress.**

143 **(A, B)** *atl-1(tm853)* knockout mutants are resistant to size reduction induced by *atp-3* or *isp-1* bacterial
144 feeding RNAi (compare 1/10th strength RNAi to vector-treated control, *panel A*). Tested worms include
145 wild type, *atm-1(gk186)* and *atl-1(tm853)* single mutants, as well as two independent *atl-1(tm853); atm-*
146 *1(gk186)* lines. Worm length is quantified in *panel B*. All worms were seeded at the same initial time.
147 Each row was photographed at a common time interval after seeding, and this time interval increased
148 with increasing RNAi potency. Evident across rows are differences in growth rates when strains are
149 cultured on the same RNAi treatment. Error bars: SEM. Significance testing: Student's t-test. Asterisks
150 refer to difference relative to respective wild type sample: **p<0.01, ***p<0.001.

151 **(C, D)** *Charts on Left*: Adult lifespan of worm strains tested in (A). Shown is a representative study. All
152 conditions were tested in parallel derived from a starting population of 16,000 synchronous eggs.
153 Replicate data for *atp-3* is presented in **Figure 2**. *Right panels*: Schematics illustrating the right-shifting
154 effect of ATL-1 removal on mean lifespan following exposure to *atp-3* and *isp-1* RNAi. Curve shapes
155 are based on the 12-point RNAi data collected in Rea *et. al.* ³⁵.

156 **(E)** RNAi knockdown efficacy is not altered in *atl-1(tm853)* mutants. mRNA levels were quantified by q-
157 RT PCR following exposure to 1/10th strength *atp-3* or *isp-1* bacterial feeding RNAi (n=3 and n=1
158 experimental replicates, respectively). Error bars: SEM. Significance testing: Student's t-test. Asterisks
159 refer to difference relative to wild type vector control **p<0.01, ***p<0.001.

160 In (A-E), all worms are unbalanced animals (~1,000) derived from F1 progeny of parents carrying the
161 nT1 reciprocal chromosomal translocation. These worms were hand selected from the 16,000 eggs

162 after they matured into adults. The wild type control line (SLR4), was deliberately moved into the nT1
163 genetic background as the appropriate control (see *Materials & Methods*).

164

165 **MAK-1 and MAK-2 participate in mitochondrial retrograde response signaling**

166 During the course of our studies we made the unexpected observation that two independently-
167 generated *atm-1(gk186); atl-1(tm853)* double mutants regained their sensitivity to *atp-3* and *isp-1*
168 knockdown (**Fig. 1**). This observation provides additional support for the notion that the RNAi
169 machinery is unaffected by loss of *atl-1*, but to explain this unexpected result, we have formed the
170 following working hypothesis: ETC disruption results in DNA damage that normally activates ATR. In
171 the absence of ATR, DNA damage accumulates, or secondary forms of DNA damage accumulate, and
172 eventually ATM is activated. In the absence of both ATR and ATM, a third checkpoint response, with a
173 higher threshold for activation, is triggered. This model reflects the well-established redundancy in the
174 DNA damage response network²². Several recent studies by us and others^{13, 36, 37}, have shown a role
175 for MAPK signaling following ETC disruption in worms. Interestingly, the p38 MAPK-activated protein
176 kinases MAPKAP-2 and MAPKAP-3 are checkpoint proteins known in humans to act in parallel to ATM
177 and ATR^{38, 39, 40}. To explore the possibility that alternate checkpoint signaling is activated in PIKK
178 mutant worms following ETC disruption, we exposed animals to *atp-3* knockdown and simultaneously
179 inhibited expression of either MAK-1 or MAK-2, the worm orthologs of MAPKAP-2 and -3, respectively.
180 The effect of these treatments on *atl-1(tm853)* and *atm-1(gk186)* single mutants, *atm-1(gk186); atl-*
181 *1(tm853)* double mutants, and wild type worms was examined. Our results can be summarized as
182 follows: (i) Knockdown of *mak-1* or *mak-2*, either alone or in combination with *atp-3* knockdown, had no
183 effect on final adult size in any of the genetic backgrounds (**Fig. 2A**). (ii) Knockdown of *mak-1* or *mak-2*
184 failed to reproducibly prevent life extension following *atp-3* inhibition in the two independent *atm-*
185 *1(gk186); atl-1(tm853)* double mutant isolates. (iii) Unexpectedly, the survival of *atl-1(tm853)* mutants
186 exposed to *atp-3* knockdown was further impaired when undertaken in conjunction with *mak-1* or *mak-*
187 *2*. A similar result was also observed for the *atm-1(gk186)* mutant. (iv) For wild type worms, only *mak-1*
188 knockdown significantly reduced *atp-3* mediated life extension (**Fig. 2B, C**). These findings suggest that

189 at least two other checkpoint proteins, namely MAK-1 and MAK-2, are causally involved in lifespan
190 extension (but not size determination) of worms experiencing mitochondrial ETC disruption. The role of
191 different checkpoint proteins is therefore dependent upon the functional status of both ATL-1 and ATM-
192 1. When the latter two proteins are disrupted simultaneously, MAK-1 and MAK-2 become dispensable,
193 potentially implying yet another checkpoint system awaits identification in *atm-1(gk186); atl-1(tm853)*
194 double mutants. Although clearly complicated, this is not unexpected for a response that is network-
195 based and sensitive to a variety of DNA lesions.

196

197 **Figure 2. MAPKAP kinases are active following mitochondrial respiratory chain stress.**

198 (A-C) The MAPKAP kinases MAK-1 and MAK-2 play no role in size control of worms exposed to 1/10th
199 strength *atp-3* feeding RNAi (A), however they do control lifespan in wild type worms, *atm-1 (gk186)*
200 mutants and *atl-1(tm853)* mutants (B, C). Worms in (A) and (B) were established independently using
201 a total of 8,000 and 32,000 synchronized eggs, respectively, and all conditions in each panel were
202 tested in parallel. In (A), all worms were photographed at the same chronological point. In (B), the
203 vertical line marks median survival of wild type worms on vector control RNAi. In (A-C), all worms were
204 the unbalanced F1 progeny of parents carrying the nT1 reciprocal chromosomal translocation.

205

206 **Knockdown of DNA pol α reverses the small phenotype of *atm-1(gk186); atl-1(tm853)* mutants**

207 To further explore the role of novel checkpoint proteins in modulating the critical ETC threshold in *atm-*
208 *1(gk186); atl-1(tm853)* double mutants, we undertook a double RNAi screen of 201 DNA damage
209 response-related genes. We asked whether knockdown of a target gene in this genetic background
210 could re-confer resistance to *atp-3* knockdown, similar to *atl-1(tm853)* mutants (for screen details see
211 **Fig. 3A**). We identified two genes: *scc-3*, which encodes a cohesin complex subunit; and Y47D3A.29,
212 which is orthologous to the human PolA1 catalytic subunit of DNA polymerase alpha (DNA pol α , **Figs.**
213 **43, C**). The effect of losing either gene was robust to three different post-hoc tests (each $p < 0.001$, see
214 **Tables S1-S3** and **Methods** for details of statistical testing; see also **File S2** for final round hit dataset).
215 Isolation of PolA1 is particularly intriguing because it suggests that *atp-3* knockdown in *atm-1(gk186);*
216 *atl-1(tm853)* double mutants could be inducing some kind of disruption to DNA, its repair, or its

217 replication and which is by-passable by low fidelity polymerases (which presumably accommodate
218 knockdown of PolA1). This in turn might avoid checkpoint activation and make animals appear more
219 *atl-1(tm853)*-like in our assay.

220

221 **Figure 3. Screen for additional checkpoint proteins activated by mitochondrial ETC dysfunction.**

222 (A) Schematic of RNAi screen used to identify DNA damage response genes active in *atl-1(tm853);*
223 *atm-1(gk186)* double mutants following *atp-3* knockdown. Test RNAi that differentially countered the
224 size reducing effect of 1/10th strength *atp-3* RNAi in unbalanced *atl-1(tm853); atm-1(gk186)* worms but
225 not nT1-containing *atl-1(tm853); atm-1(gk186)/+* worms, were sought (hit).

226 (B) Results of RNAi screen. The effect of each test RNAi on the length of unbalanced worms and nT1-
227 containing worms in the presence and absence of 1/10th strength *atp-3* RNAi is reported as a mean
228 difference ratio. The 95% confidence interval (CI) for the ratio is shown. RNAi knockdown of *scc-3* and
229 *Y47D3A.29* (labeled DNA PolA1) both significantly reduced the mean ratio relative to vector-only test
230 RNAi ($p < 0.001$, see **Methods** for significance testing procedure).

231 (C) *Top row*: Size distribution of worm populations treated with *scc-3* (*left*) or *Y47D3A.29* (*right*) feeding
232 RNAi. *Bottom row*: Histograms of mean difference ratios for worm populations treated with *scc-3* (*left*)
233 or *Y47D3A.29* (*right*) feeding RNAi and plotted relative to worms treated with vector in place of test
234 RNAi. Mean difference ratios were generated by random sampling from the distributions in the *top row*.

235

236 **No evidence for permanent nuclear DNA damage following mitochondrial ETC disruption**

237 Nuclear DNA (nDNA) damage is the canonical signal that results in activation of ATR. In worms,
238 resected ends of dsDNA breaks, and stalled replication forks, have both been shown to activate ATL-1
239 ⁴¹. Both lesions contain single-stranded DNA (ssDNA), and binding of heterotrimeric replication protein
240 A (RPA) to these regions in turn recruits and activates ATL-1. To test if ETC disruption results in
241 elevated levels of dsDNA breaks we focused on *isp-1(qm150)* genetic mutants, since no viable *atp-3*
242 mutant exists, and utilized TUNEL staining on sections of paraffin-embedded worms ⁴². We found no
243 evidence for increased nDNA breakage (**Supplemental Fig. S2A**). DNA repair is sometimes
244 inaccurate, depending on the repair machinery that is employed. To test if DNA mutation frequency was

245 increased in worms exposed to ETC disruption we employed four independent genetic assays. To
246 facilitate analysis, these studies were undertaken using *atp-3* RNAi. The eT1 (III;V) and nT1(IV;V)
247 reciprocal chromosomal translocations each suppress recombination against the regions they balance
248 (~15 Mbp for both balancers). Homozygous-lethal DNA mutations therefore accumulate on balanced
249 chromosomes and they become identifiable when eT1 and nT1 chromosomal pair are lost because
250 unbalanced progeny that are homozygous for the mutation are inviable and hence absent. Using both
251 assays, we found no evidence for increased nDNA mutation rate following knockdown of *atp-3* in wild
252 type worms (**Fig. 4A**). Similarly, use of two genetic mutation (Unc) reversion assays yielded similar
253 conclusions (**Fig. 4B**). Taken together, our data show there is neither an increase in DNA strand
254 breakage nor is there an increase in nuclear DNA mutation frequency in worms experiencing
255 mitochondrial ETC dysfunction.

256

257 **Figure 4. Nuclear DNA mutation rate is not increased following mitochondrial ETC disruption.**

258 **(A, B)** Multiple genetic screens reveal no significant increase in nuclear DNA mutation frequency
259 following knockdown of *atp-3* ($p>0.05$, Fisher's Exact Test). Phenotypes scored include lethal nuclear
260 DNA mutation events covered by the eT1 and nT1 chromosomal translocations (A), and recovery of
261 wild type movement in *unc-58(3665)* and *unc-93(e1500)* mutants (B). Knockdown of replication protein
262 A (*rpa-1*) was included as a positive control in (B).

263

264 **Ribonucleotide and deoxyribonucleotide pools are disrupted by mitochondrial ETC dysfunction**

265 To search for alternate mechanisms by which ATL-1 might be activated in worms experiencing
266 mitochondrial ETC dysfunction, we examined changes in whole-worm nucleotide levels. As in humans,
267 pyrimidine biosynthesis in *C. elegans* requires a functional mitochondrial electron transport chain. This
268 is because formation of orotate from dihydroorotate is coupled to reduction of ubiquinone (UQ) in a
269 reaction catalyzed by the inner mitochondrial membrane enzyme dihydroorotate dehydrogenase
270 (DHODH, **Supplemental Fig. S3**). In mammals, processes that slow flux through the mitochondrial
271 ETC, downstream of UQ, also slow the rate of dihydroorotate dehydrogenase resulting in measurable
272 disruption of nucleotide pools⁴³. Several important enzymes are sensitive to changes in nucleotide

273 abundance, including DNA polymerases which are rate-limited by availability of their
274 deoxyribonucleotide substrates⁴⁴. Stalling of DNA polymerase, followed by continued DNA unwinding
275 by the MCM helicase, results in ssDNA formation^{45,46}, which is a known substrate for ATR activation.

276

277 To measure nucleotide levels, we re-focused our attention on the *isp-1(qm150)* genetic mutant for ease
278 of culture. We interrogated three stages of development – the final two stages of larval development
279 (L3 and L4) and the first day of adulthood. These stages were selected because in wild type worms
280 there is a heavy demand for nucleotide precursors around the L3/L4 molt, and then again around the
281 L4/adult molt. At these times the gonad arms are expanding and there is also a concomitant five-fold
282 and a 6-fold increase in mitochondrial DNA (mtDNA), respectively⁴⁷. Among nine deoxyribonucleotide
283 species that we were able to resolve and reliably detect (see **Methods**) we observed significant
284 increases in dCDP and dTMP in L4 larvae of *isp-1(qm150)* mutants (**Fig. 5A**). The increase in dCDP
285 abundance was maintained into adulthood (**Fig. 5B**). Among eleven ribonucleotide species that we
286 were able to reliably resolve and detect, we observed significant increases in AMP, CMP and UMP in
287 L4 larvae of *isp-1(qm150)* mutants (**Fig. 5C**). This was accompanied by a significant decrease in the
288 level of GTP. In adult *isp-1(qm150)* worms, changes in ribonucleotide pools became more pronounced,
289 with eight species being significantly underrepresented – ADP, ATP, GDP, GTP, CMP, CTP, UDP, UTP
290 (**Fig. 5D**). Changes in nucleotide pools were specific to L4 and adult worms since we did not detect any
291 measureable differences in any quantifiable nucleotide species in L3 larvae of *isp-1(qm150)* mutants
292 relative to wild type worms (**Fig. 5E**). Finally, the absence of a corresponding increase in many of the
293 monophosphate ribonucleotide species in adult *isp-1(qm150)* worms when their corresponding di- and
294 triphosphate counterparts decreased, suggests ribonucleotide pool sizes are reduced in these animals.
295 We combined the levels of each mono-, di- and triphosphate species and tested if they differed
296 significantly between strains at each developmental stage, but they did not. Error propagation,
297 however, severely reduced our statistical resolving power (**Fig. 5F**). Collectively, we conclude that
298 disruption of the mitochondrial ETC in *C. elegans* results in measurable and significant changes in the

299 abundance of multiple nucleotide species, notably with all ribonucleotide triphosphate species
300 becoming underrepresented by adulthood.

301

302 **Figure 5. Ribonucleotide and deoxyribonucleotide pool ratios are disrupted following**
303 **mitochondrial ETC disruption.**

304 (A-E) Absolute levels of deoxyribonucleotide (A and C) and ribonucleotide (B and D) species in wild
305 type (N2) and *isp-1(qm150)* worms at the L4 and day-one adult stages, measured using
306 quantitative LC-MS. Red asterisks indicate nucleotide quantities that differ significantly between strains
307 (Student's t-test, 5% FDR). Four nucleotides were not measurable by our assay (dGMP, dGDP, dGTP,
308 GMP). No significant differences in any nucleotide level existed between strains at the L3 larval stage
309 (E).

310 (F) Relative nucleotide pool sizes in L3, L4 and day-one adult N2 and *isp-1(qm150)* worms, determined
311 by summing together the mono-, di- and triphosphate species of each deoxyribonucleotide or
312 ribonucleotide (guanosine was an exception) and normalizing to dCNP or CNP, respectively, across
313 each larval stage. No significance difference in each respective nucleotide pool size between strains
314 was detected (Student's t-test, 5% FDR; N = 3, 7 and 3 experimental replicates for N2 L3, L4,
315 and adult worms; and N= 3, 5 and 3 for *isp-1(qm150)* L3, L4 and adult worms, respectively).

316

317 **Evidence for RNA polymerase stalling following mitochondrial ETC disruption**

318 Stalling of RNA polymerase II (RNA pol II) during transcription is sufficient to activate an ATR, RPA and
319 p53-dependent DNA damage response in human fibroblasts ⁴⁸. Given that mitochondrial ETC
320 dysfunction in *isp-1(qm150)* mutants leads to measurable reductions in all four ribonucleotide
321 triphosphates, and because we have previously shown a role for p53/*cep-1* in the life extension of
322 these worms ¹⁹, we hypothesized that ATL-1 activation following ETC disruption might occur as a result
323 of RNA pol II stalling due to reduced nucleotide availability. We therefore quantified the formation of R-
324 loops on genomic DNA ⁴⁹. R-loops are DNA:RNA hybrids that accumulate when transcription stalls
325 (Fig. 6A). We detected R-loops in purified, whole-worm genomic DNA fractions using slot blot analysis
326 in conjunction with a DNA:RNA hybrid-specific antibody (α S9.6) ⁵⁰. To obtain sufficient material for

327 these studies we utilized a double feeding RNAi approach and tested four conditions: Wild type worms
328 exposed to either vector control RNAi, 1/10th strength *isp-1* RNAi, 9/10th strength *atl-1* RNAi, or both
329 9/10th strength *atl-1* RNAi with 1/10th strength *isp-1* RNAi. Vector control feeding RNAi was added as
330 balancer where appropriate. qRT-PCR analysis undertaken before the start of the experiment revealed
331 9/10th strength *atl-1* RNAi reduced *atl-1* mRNA by 50% (**Fig. 6B**), the same amount that was observed
332 in maternal-effect rescued *atl-1(tm853)* mutants (**Fig. 6C**). The results of our R-loop studies can be
333 summarized as follows (**Fig. 6D**): Knockdown of *isp-1* significantly enhanced R-loop formation relative
334 to vector control (Student's t-test, $p < 0.05$). As predicted, *isp-1* functioned epistatically to *atl-1*, since *atl-*
335 *1* knockdown did not block R-loop formation by *isp-1*, as would be expected for a gene that functioned
336 downstream of R-loop accumulation. We next tested whether any differences in DNA:RNA polymer
337 length distinguished R-loops generated in worms exposed to *isp-1* RNAi from those exposed to *isp-1*
338 and *atl-1* double RNAi. Genomic fractions were separated on an agarose gel, stained with ethidium
339 bromide, then transferred to nitrocellulose and probed with α S9.6 antibody (**Fig. 6E**). No overt
340 difference distinguished the two samples, however in both instances we noted some of the staining with
341 α S9.6 localized to low molecular weight DNA:RNA fragments ($< 2\text{kb}$), in addition to the higher
342 molecular weight structures that we expected. The identity of these smaller fragments remains
343 uncharacterized (see **Discussion**). Collectively, our studies suggest that transcriptional stalling is
344 increased in worms exposed to mitochondrial ETC disruption, identifying one route by which ATL-1 is
345 potentially activated in these animals.

346

347 **Figure 6. Evidence for RNA Pol II stalling following mitochondrial ETC stress.**

348 (A) Schematic showing genesis of R-loops following stalling of RNA Polymerase II. Modified from ⁵¹.

349 (B, C) RNAi knockdown of *atl-1* in wild type (N2) worms reduces *atl-1* transcript abundance to the same
350 extent as in maternal-effect *atl-1(tm853)* mutants. In (C), all worms are unbalanced F1 progeny from
351 parents carrying the nT1 reciprocal chromosomal translocation ($N = 3$; error bars: SEM; significance
352 testing: Student's t-test; symbols: significantly different from wt: * $p < 0.05$; *** $p < 0.001$; significantly
353 different from *atl-1(tm853)*: $\wedge p < 0.05$). In (B), $N=2$ and # marks range.

354 (D) R-loops are significantly increased in N2 worms following knockdown of *isp-1* (1/10th RNAi
355 strength). Combined knockdown of *isp-1* (1/10th RNAi strength) and *atl-1* (9/10th RNAi strength) does
356 not abrogate R-loop accumulation. *Top panel*: representative immunoblot of R-loops, *Bottom panel*:
357 Immunoblot quantitation: $N = 3$; *error bars*: SEM; Student's t-test (vs. vector): * $p \leq 0.05$, ** $p \leq 0.01$.
358 (E) Samples in (D) were further analyzed by agarose gel electrophoresis (*top two panels*) and then
359 western blotting using an antibody that cross reacts with DNA::RNA hybrids (α S9.6, *bottom panel*).
360 Knockdown of *isp-1* results in an increase of gDNA associated R-loops, and unknown small molecular
361 weight DNA::RNA hybrids.

362

363 **RNA splicing is not altered by mitochondrial ETC disruption**

364 Having identified a possible mechanism by which ATL-1 is activated in worms experiencing
365 mitochondrial ETC stress, we next sought to determine the mode by which ATL-1 acts to further disrupt
366 mitochondrial function. It is well-established that pre-mRNA splicing is a co-transcriptional process⁵²
367 and it has also been reported that *isp-1(qm150)* mutants are sensitive to knockdown of two
368 spliceosome factors SFA-1 and REPO-1, fully ablating their life extension⁵³. We therefore tested
369 whether stalling of RNA pol II altered either splicing efficiency or splicing fidelity in worms exposed to
370 ETC disruption, and if ATL-1 played a role in this process. We used two synthetic-gene reporter assays
371 developed by Kuroyanagi and colleagues^{54,55} designed to measure alternate splicing at the *egl-15* and
372 *ret-1* loci, respectively. The latter reporter was shown to be a sensitive marker of age-related splicing
373 dysfunction⁵³. Each assay has the potential to produce two fluorescent outputs that record changes in
374 the nature of a differential splicing event and the tissues in which these events occur (**Supplemental**
375 **Fig. S4 A, B**). We exposed worms carrying the relevant reporter cassette to double feeding RNAi
376 targeting *atp-3* or *isp-1* (1/10th strength) in conjunction with either *atl-1* or vector control (9/10th RNAi
377 strength) (**Supplemental Fig. S4C**). Animals were followed three days into adulthood. None of the
378 conditions that disrupted the mitochondrial ETC, neither in the presence or absence of *atl-1*, resulted in
379 alteration of *egl-15* or *ret-1* splicing relative to vector control treated animals.

380

381 **Reduced ATL-1 activity does not enhance hormetic stress response activation**

382 We next tested whether loss of *atf-1* affected the activity of major stress response pathways known to
383 be activated by *atp-3* or *isp-1* depletion^{13, 35, 56 3}. Loss of *atf-1* did not result in constitutive activation of
384 *Phsp-6::GFP*, *Pgst-4::GFP* or *Ptbb-6::GFP*, which are markers of ATFS-1, SKN-1/NRF-2 and PMK-
385 3/p38 activation, respectively (**Supplemental Fig. S5A-D**). Neither did loss of *atf-1* increase gene
386 expression of *sod-3*, *ugt-61* or *hsp-6* (**Supplemental Fig. S5E**). These results indicate that reduction of
387 *atf-1* does not affect typical mitochondrial stress response pathways.

388

389 **Oxygen consumption remains surprisingly unaltered in *atf-1* mutants exposed to ETC disruption**

390 We next tested whether mitochondria in *atf-1(tm853)* mutants were inherently different from those of
391 wild type worms. We also analyzed mitochondria from *atm-1(gk186)* single mutant worms, as well as
392 *atf-1(tm853); atm-1(gk186)* double mutants. Properties that we examined included mitochondrial DNA
393 (mtDNA) content, nuclear-encoded ETC transcript abundance, mitochondrial morphology and whole-
394 worm oxygen consumption. Our findings can be summarized as follows: relative to wild type worms,
395 mtDNA copy number is halved in *atf-1(tm853)* mutants, consistent with an earlier report⁵⁷. mtDNA
396 content was also halved in *atf-1(tm853); atm-1(gk186)* double mutants (**Fig. 7A**). To assess changes in
397 nuclear-encoded ETC transcript abundance, we focused on five genes: *nuo-6*, *mev-1*, *isp-1*, *cco-1* and
398 *atp-3*, representing subunits from mitochondrial complexes I through V, respectively. We found that all
399 transcripts except *nuo-6* were significantly decreased relative to wild type worms in all four mutant
400 strains studied. The only exception was *mev-1*, for which mRNA levels remained unchanged in *atm-*
401 *1(gk186)* mutants (**Fig. 7B**).

402 To quantify changes in mitochondrial morphology we employed a hexokinase-2::GFP
403 translational reporter (HXK2::GFP) that is localized to the outer mitochondrial membrane⁵⁸. We
404 observed a significant increase in the number of fused mitochondria in reporter worms treated with *isp-*
405 *1* RNAi (p<0.0024, see **Methods** for details of statistical testing). Co-knockdown of *atf-1* did not
406 significantly affect this result. Mitochondria in worms treated only with *atf-1* RNAi were indistinguishable
407 from those of wild type animals (**Fig. 7C**). Finally, the most significant finding that we uncovered related
408 to alterations in oxygen consumption by *atf-1(tm853)* mutants. When wild type worms, *atf-1(tm853)* and

409 *atm-1(gk186)* single mutants, as well as *atl-1(tm853); atm-1(gk186)* double mutants were cultured on
410 *isp-1* RNAi, the basal oxygen consumption rate of *atl-1(tm853)* mutants, as well as *atl-1(tm853); atm-*
411 *1(gk186)* double mutants, significantly increased relative to wild type worms (**Fig. 7D**). Moreover, while
412 *isp-1* knockdown uniformly decreased oxygen consumption in wild type worms, *atm-1(gk186)* single
413 mutants and *atl-1(tm853); atm-1(gk186)* double mutants, and by the same extent, oxygen consumption
414 in *atl-1(tm853)* surprisingly remained unchanged following this treatment. We conclude that while *atl-*
415 *1(tm853)* mutants contain half as much mtDNA as wild type worms and have reduced abundance of
416 several nuclear-encoded ETC transcripts, these worms surprisingly maintain normal oxygen
417 consumption, even when confronted with disruption of their mitochondrial electron transport chain.

418

419 **Figure 7. *atl-1(tm853)* mutants maintain normal oxygen consumption when confronted with**
420 **disruption of their mitochondrial ETC.**

421 (A) Mitochondrial DNA abundance is significantly decreased in *atl-1(tm853)* mutants compared to wild
422 type worms (N=3).

423 (B) Transcript abundance of nuclear-encoded ETC genes is significantly decreased in *atl-*
424 *1(tm853)* mutants relative to wild type worms (N=3; Cx: complex).

425 (C) Morphology of body-wall muscle mitochondria assessed using HXK-2::GFP⁵⁸, following *atl-1*
426 knockdown in the absence or presence of mitochondrial ETC disruption (1/10th strength *isp-1* RNAi).
427 Both *atl-1* and *isp-1* knockdown significantly alter mitochondrial morphology relative to vector-control
428 (p<0.0024, refer to **Methods** for significance testing).

429 (D) *atl-1(tm853)* mutants are resistant to changes in oxygen consumption following *isp-1* knockdown
430 (1/10th strength RNAi). All other tested strains experienced a significant decrease in oxygen
431 consumption (N=4). Oxygen consumption was measured using a Seahorse XFe24 Analyzer.

432 In (A) and (D), all worms are the unbalanced F1 progeny of parents carrying the nT1 reciprocal
433 chromosomal translocation. In (A), (B) and (D), asterisks indicate significantly different from wild type
434 (Student's t-test) unless otherwise noted by a bar for the relevant comparison group: * p<0.05. **
435 p<0.01. *** p<0.001; ns, not significant. In (D), ^^ p<0.001 in comparison to wild type on *isp-1* RNAi. In
436 (A) and (B), error bars are SEM; in (D), box and whisker plots show 10-90 percentile, with outliers
437 marked (dots).

438

439 **Loss of ATR leads to recovery of translational activity in worms exposed to ETC disruption.**

440 Several mechanisms could explain how *atl-1(tm853)* mutants maintain oxygen consumption despite
441 ETC disruption. Any process that ultimately increases flux or efficiency of the respiratory chain could be
442 involved. Enhanced supercomplex formation, elevated matrix Ca^{2+} , modification of ETC subunits, or
443 simply enhanced translational output of respiratory subunits, could all be behind the unique respiratory
444 response seen in *atl-1(tm853)* mutants. We focused on translational output because there is evidence
445 from human 293T cells that ATR might directly regulate the ribosomal machinery by affecting
446 phosphorylation of the nascent polypeptide-associated complex (NAC)²². In worms, ICD-1 is the sole
447 β NAC isoform^{59, 60}. Although the ATR phosphorylation site of human BTF3/ β NAC is not conserved in
448 ICD-1, we observed by western analysis that ICD-1 protein levels are selectively elevated in *atl-*
449 *1(tm853)* mutants following *atp-3* knockdown (*isp-1* knockdown was not tested due to limited quantities
450 of antisera, see Materials & Methods) (**Fig. 8A**). Moreover, early analyses involving several hundred
451 microarray datasets⁶¹ showed *icd-1* formed part of a tightly clustered gene co-expression group (**Fig.**
452 **8B**) that is significantly enriched (hypergeometric distribution, $p < 0.05$) for genes encoding ribosomal
453 and mitochondrial ETC subunits, as well as key translational regulatory factors (**Fig. 8C**). We therefore
454 tested whether global translational activity was downregulated by mitochondrial ETC disruption and if
455 loss of *atl-1* permitted its recovery. We employed polysome profiling in conjunction with RNAi targeting
456 both *isp-1* (1/10th RNAi strength) and either *atl-1* or vector (both at 9/10th RNAi strength). We found that
457 the actively translating polysome fraction of worms treated with *isp-1* RNAi was decreased by half
458 relative to vector control-treated worms. Strikingly, simultaneous removal of both *atl-1* and *isp-1*
459 restored polysome activity to wild type levels (**Fig. 8D**). Loss of *atl-1* in the absence of ETC disruption
460 did not significantly impact polysome abundance relative to wild type worms. These data imply that
461 ATL-1, when activated by mitochondrial ETC disruption, normally acts to dampen global ribosomal
462 translation. Whether this is through a novel phosphorylation site on ICD-1, downregulation of factors
463 that normally control *icd-1* expression, or via some other means that globally regulates translational
464 activity, remains unclear. There must be some specificity in the translational targets of ATR-1, however,

465 because simply elevating global rRNA production by inhibiting *ncl-1*, a negative regulator of FIB-
466 1/fibrillarin, a nucleolar protein involved in the regulation and maturation of rRNA, is not sufficient to
467 block the size reduction caused by *isp-1* bacterial feeding RNAi (**Fig. 6E, F**). Collectively, our results
468 lead to a model for how ATL-1 acts to modulate the mitochondrial threshold effect (**Fig. 8G**).

469 **Figure 8. Knockdown of *atl-1* prevents global translation reduction caused by mitochondrial ETC**
470 **disruption.**

471 (A) *Top panel*: ICD-1 protein abundance in *atl-1(tm853)* mutants relative to wild type animals following
472 *atp-3* knockdown (N=2, bars indicate *range*). *Bottom panel*: Representative western blot. All worms are
473 the unbalanced F1 progeny of parents carrying the nT1 reciprocal chromosomal translocation.

474 (B) *C. elegans* gene co-expression terrain map generated using VxInsight⁶¹ showing *icd-1*-containing
475 'Mount 23' (*white arrow*). Progressive zoom shots of Mount 23 are shown (*top to bottom*). The position
476 of *icd-1* is marked by a *white square*.

477 (C) 88 of 133 (66%) genes comprising Mount 23 of the *C. elegans* gene co-expression terrain map
478 encode either mitochondrial ETC proteins or ribosomal proteins, including both α - and β -NAC (ICD-1).

479 (D) Polysome profiling shows knockdown of *atl-1* (9/10th RNAi strength) restores the level of actively
480 translating ribosomes to control levels in worms grown on *isp-1* RNAi (1/10th strength).

481 (E) *ncl-1(e1865)* and *ncl-1(e1942)* mutants do not confer resistance to the size reducing effects of
482 bacterial feeding RNAi targeting *isp-1* relative to wild type (N2) worms. *ncl-1* mutants are naturally
483 larger than N2 worms. (mean +/- SEM)

484 (F) RNAi remains efficacious in *ncl-1(e1865)* and *ncl-1(e1942)* mutants. Shown is survival following
485 exposure to increasing doses of a lethal feeding RNAi (*skn-1*). Data from a single experiment is shown
486 that was established simultaneously with common reagents and using 20 synchronous one day old
487 adult worms per test condition.

488 (G) Model showing how removal of ATL-1 counters loss of mitochondrial electron transport chain
489 disruption. ETC insufficiency results in nucleotide imbalances, stalling of nucleotide polymerases,
490 activation of ATL-1, and dampening of global translation, leading to magnification of ETC dysfunction.

491

492 **DISCUSSION**

493 In this study, we discovered that the PIKK kinase ATR/ATL-1 plays a specific role in modulating the
494 mitochondrial threshold effect of *C. elegans*. When flux through the ETC was reduced, ATL-1 was
495 activated. We presented data suggesting stalling of RNA polymerase could be the trigger for ATL-1
496 activation. We recorded measurable reductions in many nucleotide species in adult worms, including
497 substrates for both RNA and DNA polymerase, and we presented biochemical evidence showing RNA
498 polymerase stalling following ETC disruption. In addition to these findings we showed that ATL-1
499 paradoxically exacerbates mitochondrial dysfunction during times of mitochondrial stress. Specifically,
500 when worms containing reduced levels of *atl-1* were challenged with ETC disruption, unlike wild type
501 animals, these showed no signs of impairment in global translational output or respiratory oxygen
502 consumption. Phenotypically, loss of *atl-1* effectively reversed a mitochondrial ETC insufficiency in *C.*
503 *elegans*. The survival benefits of further dampening ETC activity following an ETC insult are not entirely
504 clear, but dampening of mitochondrial respiratory activity in conjunction with global translational
505 dampening might represent an effort to slow overall metabolism or to maintain stoichiometric balance
506 between nuclear- and mitochondria-encoded ETC proteins⁶².

507 **Mode of ATL-1 Activation Following Mitochondrial ETC Disruption**

508 In our search for signals that triggered ATL-1 activation in response to ETC disruption we found no
509 evidence for elevated rates of nuclear DNA mutation or strand breakage. This does not preclude the
510 possibility that DNA damage occurred and was accurately repaired. Such damage would have escaped
511 detection in our assays. Nonetheless, we investigated other potential mechanisms of ATL-1 activation
512 and found that nucleotide pools were significantly changed when analyzing *isp-1(qm150)* mutants. This
513 is significant because ATR activation has been linked to changes in nucleotide pools in other model
514 systems. Specifically, in *S. cerevisiae*, glucose starvation induces Snf1p (AMPK) at the mitochondrial
515 surface following reduction of adenosine ribonucleotide energy charge. In turn, Snf1p was shown to
516 phosphorylate Mec1p (ATR)³⁴. Whether a similar mode of ATR activation functions in *C. elegans*
517 remains unclear, but Ggc1p, the protein that initially recruits Mec1p to the yeast mitochondrial
518 membrane under low glucose conditions has no worm ortholog. We therefore decided to pursue an

519 alternate hypothesis for nucleotide-dependent activation of ATR in worms, namely stalling of RNA
520 and/or DNA polymerases.

521 Previously it had been shown that blocking RNA polymerase during transcriptional elongation is
522 sufficient to activate ATR and induce a DNA damage response (DDR)⁴⁸. Indeed, we found evidence
523 that DNA::RNA R-loop hybrids are increased in the presence of mitochondrial ETC disruption, which is
524 indicative of transcriptional stalling. However, it is unclear whether all the R-loops we detected were
525 genomic DNA (gDNA)-derived transcription intermediates. When examining samples on an agarose gel
526 in conjunction with an antibody targeting these structures (S9.6), R-loops are expected to appear at a
527 high molecular weight in association with the gDNA band. We clearly detected an elevated signal in this
528 region in our *isp-1* RNAi treated samples, consistent with our hypothesis. Also but, we observed an
529 additional smear of low molecular weight nucleic acids. At this point it is unknown if these low molecular
530 weight molecules are truly DNA::RNA hybrids or a contaminating nucleic acid. The S9.6 antibody has a
531 5-fold higher affinity for DNA::RNA hybrids over RNA::RNA hybrids⁵⁰, so in anticipation of the latter our
532 samples were treated with RNase A ruling out this possibility. One idea is that the low molecular weight
533 DNA::RNA hybrids are derived from mtDNA fragments that have leaked from dysfunctional
534 mitochondria. Consistent with this idea, in mouse embryonic fibroblasts, mitochondrial stress results in
535 mtDNA leaking into the cytoplasm and initiating an immune response⁶³. On the other hand, worms use
536 a rolling circle replication method for their mtDNA, so precisely how R-loops would form in the absence
537 of D-loop (theta) replication, as is used by mammalian cells, remains enigmatic⁶⁴. Another idea is that
538 the low molecular weight species we detected are cytoplasmic DNA::RNA hybrids produced by DNA
539 polymerase α (DNA pol α). Starokadomsky and colleagues⁶⁵, showed that a small fraction of DNA pol α
540 localizes to the cytoplasm in human cells where it generates DNA::RNA hybrids. These molecules
541 directly modulate production of type I interferons and possibly exist to control the activation threshold of
542 the innate immune response by foreign nucleic acids. In patients with X-linked reticulate pigmentary
543 disorder (XLPDR), a primary immunodeficiency with autoinflammatory features, levels of the catalytic
544 subunit of DNA pol α (DNA PolA1) are decreased enough to disrupt cytoplasmic DNA::RNA hybrid
545 formation, but not enough to affect DNA replication⁶⁵. Intriguingly, in our screen for DDR proteins that

546 when inhibited reversed the small size phenotype of *atl-1(tm853); atm-1(gk186)* double mutants
547 experiencing mitochondrial ETC stress, we identified an RNAi clone targeting DNA PolA1. Although not
548 discussed earlier, we also isolated a second DNA pol α clone in that screen that targeted a different
549 region of DNA PolA1 but instead resulted in synthetic lethality. This dose-dependent phenotypic
550 response is remarkably similar to what was just discussed for humans. Obviously, more work is needed
551 to determine the identity, provenance and significance of the low molecular weight DNA:RNA species
552 in worms experiencing ETC stress and if and how they might relate to ATR activation.

553

554 **Downstream targets of ATL-1 that Modulate Mitochondrial ETC Activity**

555 One important finding from our study is the observation that *atl-1* knockdown mitigates the effects of
556 mitochondrial ETC dysfunction. This is an intriguing finding as it suggests the normal cellular response
557 to ETC disruption is ostensibly further detrimental. Two possible explanations for how loss of *atl-1* could
558 result in enhanced ETC function are, *atl-1* knockdown triggers active restoration of mitochondrial
559 function, or alternatively, *atl-1* knockdown precludes propagation of whatever negative downstream
560 effects are normally elicited by ETC disruption. According to our data, *atl-1(tm853)* mutants contain half
561 the amount of mtDNA as wild type worms and have significantly reduced abundance of nuclear-
562 encoded ETC transcripts. These findings argue against the first hypothesis. Surprisingly, despite their
563 shortcomings, we find that *atl-1(tm853)* mutants are still able to maintain oxygen consumption at near
564 normal levels when confronted with ETC disruption. The precise mechanism involved is yet to be
565 determined, but it may be as simple as *atl-1(tm853)* mutants being able to maintain the translation of a
566 factor that enhances supercomplex formation, for example⁶⁶. Alternatively *atl-1(tm853)* mutants may
567 be able to keep their cells fortified with sufficient ETC proteins to counteract any rapid turnover that is
568 likely to occur when subunits become rate-limiting during the assembly process. Along these lines,
569 when we examined polysome formation under conditions of ETC dysfunction, we found that animals
570 with functional ATL-1 had reduced polysome formation but removal of *atl-1* restored this number back
571 to pre-ETC disruption levels. Future studies will be aimed at determining the precise mRNA species
572 present in these polysomes.

573 Another way in which *atl-1(tm853)* mutants might be able to counter ETC disruption involves the
574 nascent protein folding machinery. We showed that ICD-1/ β NAC, a protein that acts as a ribosome-
575 associated chaperone, is upregulated in *atl-1* mutants upon ETC disruption. In yeast and plants, β NAC
576 plays a role in targeting proteins to the mitochondria and is required for efficient mitochondrial function
577 ^{67, 68, 69, 70, 71}. β NAC was also one of the few proteins found to be specifically regulated by ATR-dependent
578 phosphorylation in mammals ²². The ATR-dependent phosphorylation site in mammals is not conserved
579 in *C. elegans*, however there are several other potential phosphorylation sites in the ICD-1 protein
580 sequence ⁷². It will be of particular interest in future to ascertain if ATR directly regulates β NAC
581 abundance on ribosomes to modulate translation of ETC transcripts in worms.

582

583 **Mitochondrial Dysfunction in Mammals**

584 Johnson and colleagues ⁷³ successfully extended the survival of a mouse model of Leigh syndrome,
585 which was deficient in Ndufs4 of complex I, by chronic administration of the mTOR inhibitor rapamycin.
586 mTOR is a positive regulator of p70S6 kinase and a negative regulator of 4E-BP, both of which work to
587 elevate translation. At first this seems surprising in light of our findings suggesting global translation
588 needs to be elevated to counter ETC dysfunction in worms. However, while acute inhibition of mTOR
589 indeed results in global dampening of translation, it also results in the specific translational upregulation
590 of mitochondrial ETC components ^{74, 75}. Also, it has been reported that in contrast to acute rapamycin
591 administration, chronic rapamycin administration does not lead to reduced ribosomal activity *in vivo* ⁷⁶.
592 Whether the increase in polysomes that we observed in *atl-1* animals exposed to ETC disruption
593 represented upregulation of global mRNA translation or just a discrete subset of mRNAs only encoding
594 ETC proteins, remains to be determined.

595 In conclusion, we have shown that blockade of *atl-1* effectively reverses ETC disruption in *C.*
596 *elegans*. Preventing mitochondria from transitioning into their critical ETC threshold appears, quite
597 literally, to be the difference between life and death.

598

599 **METHODS**

600 A detailed description of all methods is provided in **Supplemental File S1**.

601 **Nematode Strains and Maintenance.** Genotypic information for all strains used in this study is
602 provided in **Table S4**. Lines were maintained at 20°C on standard NGM agar plates seeded with *E. coli*
603 (OP50)⁷⁷. To control for possible untoward effects derived from the *nT1(IV:V)* chromosomal pair in
604 maternally-rescued *atl-1(tm853)* mutants, all lines, including the wild type control, were moved into the
605 *nT1(IV:V)* background and then unbalanced F1 animals freshly collected for each relevant experiment.
606 Further details are provided in **Supplemental File S1**.

607

608 **Bacterial Feeding RNAi.** All bacterial feeding RNAi constructs were designed in the pL4440 vector
609 backbone and maintained in HT115 bacteria⁷⁸. Growth rate, life span, RNAi efficacy assays and RNAi
610 dilution methods are described in **Supplemental File S1**.

611

612 **Microscopy.** Images of fluorescent worms were captured using an Olympus SZX16 fluorescence
613 microscope connected to an Olympus DP71 CCD camera. In **Fig. 7C**, to determine whether differences
614 existed in the morphology of mitochondria between the four tested conditions, four randomly selected
615 images from each condition were mixed and then grouped by a scorer who was blind to image identity.
616 In a set of 16 images, 10 were co-grouped correctly. The probability that this grouping occurred by
617 chance was modeled using an Excel VBA macro that randomly binned the images into four groups of
618 four, 10,000 times (**File S3**). The final *p-value* was <0.0024 and deemed significant.

619

620 **mRNA and mtDNA Quantitation.** For quantitation of mRNA, fold change in each mRNA of interest
621 was determined using the $\Delta\Delta C_t$ method normalized to the geometric mean of *cdc-42*, *pmp-3*, and
622 *Y45F10D.4*⁷⁹. For quantitation of mitochondrial DNA (mtDNA), PCR primer pairs targeting mtDNA-
623 encoded *ctb-1* and intron 4 of genomic DNA-encoded *ama-1* were used as described⁸⁰. The ratio of
624 mitochondrial DNA to nuclear DNA was then calculated using Real Time PCR, using *ama-1* as the
625 normalizing quantity⁸¹. A complete list of qPCR primers is provided in **Table S5**.

626

627 **Mutation Screening Assays:**

628 Full methodological details of the *unc-93(e1500)* and *unc-58(e665)* reversion assays, the eT1(III;V) and
629 nT1(IV;V) lethal mutation assays, the Lac-Z Frameshift Assay, and the 'terminal deoxynucleotidyl
630 transferase dUTP nick end labeling' (TUNEL) assay are presented in **Supplemental File S1**.

631

632 **Nucleotide Extraction and Mass Spectrometry.** Quantitation of deoxyribonucleotide and
633 ribonucleotide species in whole-worm extracts of *isp-1(qm150)* and wild-type (N2) animals was
634 undertaken using HPLC-MS at the UTHSCA Mass Spectrometry Facility. Methods for nucleotide
635 extraction, separation, quantitation and statistical analysis are provided in **Supplemental File S1**.

636

637 **R-loop Quantification.** R-loop formation in worms was quantified using α S9.6 primary antibody
638 (Kerafast, 1:2000 in 5% Blotto, 16 hours, 4°C), previously shown to be selective for DNA::RNA hybrids
639 ⁵⁰. A list of western reagents and methods are provided in **Supplemental File S1**.

640

641 **Spliceosome Reporter Assays.** *egl-15* and *ret-1* alternate splicing reporter genes were engineered by
642 Kuroyanagi and colleagues ^{55, 82}. Details of reporter construction and their use is provided in
643 **Supplemental File S1**.

644

645 **Nematode Oxygen Consumption:**

646 Nematode oxygen consumption measurements were undertaken using a Seahorse XFe24 Analyzer
647 Approximately 30 worms were added to each Seahorse well, with 5 replicate wells employed per test
648 condition. We followed the procedure of Luz and colleagues ⁸³, and only averaged oxygen consumption
649 rates across the final four measurement phases for each well to provide a single rate value for that well.
650 A total of four independent experiments was performed. Significance testing was undertaken using the
651 Student's t-test, with $p < 0.05$ considered significant.

652

653 **Polysome Profiling.** Quantitative polysome profiling was undertaken using the procedure of Steffen
654 and colleagues⁸⁴ using a Brandel BR-188 Density Gradient Fractionation System. Several
655 modifications were included to optimize for *C. elegans* polysome extraction and these are described in
656 detail in **Supplemental File S1**. Two fully independent experimental replicates were collected.

657

658 **Western Analysis.** Western blotting reagents and suppliers are described in **Supplemental File S1**.

659

660 **DNA Damage Response (DDR) Screen.**

661 The *atm-1(gk186); atl-1(tm853)* suppressor screen was undertaken using a bacterial feeding RNAi
662 targeting 201 DDR-related genes⁸⁵. A detailed protocol of our screening method, including quantitation
663 of the RNAi Effect Size and Significance Testing, is provided in **Supplemental File S1** and **Tables S1-**
664 **S3**.

665

666 **FUNDING**

667 Financial support was provided by the National Institutes of Health [AG-047561 (SLR), AG025207
668 (SLR) and AG-055820 (SLR). Funding sources had no role in study design, data collection and
669 analysis, the decision to publish, or preparation of the manuscript.

670

671 **ACKNOWLEDGEMENTS**

672 We thank the following people: Dr. Hidehito Kuroyanagi (Tokyo Medical and Dental University) for the
673 splice reporters; Dr. Joel Rothman (UCSB) for the *icd-1* antibody; Alison Kell (CU, Boulder) for
674 assistance with DDR library construction; Oxana Radetskaya (UW) for critical reading of the
675 manuscript. Technical assistance was provided by Rebecca Lane, Carlos Galeano, Yvonne Penrod,
676 Haley Beam, Bill Swan and Melissa Ligon (all UT Health San Antonio). Some strains were provided by

677 the *Caenorhabditis* Genetic Stock Center, which is funded by NIH Office of Research Infrastructure
678 Programs (P40 OD010440). We also thank Wormbase.

679

680 REFERENCES

- 681 1. Schaefer AM, Taylor RW, Turnbull DM, Chinnery PF. The epidemiology of mitochondrial disorders--past,
682 present and future. *Biochim Biophys Acta* 2004, **1659**(2-3): 115-120.
- 683
684 2. Li MX, Dewson G. Mitochondria and apoptosis: emerging concepts. *F1000Prime Rep* 2015, **7**: 42.
- 685
686 3. Liu Y, Samuel BS, Breen PC, Ruvkun G. *Caenorhabditis elegans* pathways that surveil and defend
687 mitochondria. *Nature* 2014, **508**(7496): 406-410.
- 688
689 4. Khutornenko AA, Roudko VV, Chernyak BV, Vartapetian AB, Chumakov PM, Evstafieva AG. Pyrimidine
690 biosynthesis links mitochondrial respiration to the p53 pathway. *Proc Natl Acad Sci U S A* 2010, **107**(29):
691 12828-12833.
- 692
693 5. Wallace DC. Mitochondrial DNA mutations in disease and aging. *Environ Mol Mutagen* 2010, **51**(5): 440-
694 450.
- 695
696 6. Wallace DC. Mitochondria and cancer. *Nat Rev Cancer* 2012, **12**(10): 685-698.
- 697
698 7. Lane RK, Hilsabeck T, Rea SL. The role of mitochondrial dysfunction in age-related diseases. *Biochim*
699 *Biophys Acta* 2015.
- 700
701 8. Rossignol R, Faustin B, Rocher C, Malgat M, Mazat JP, Letellier T. Mitochondrial threshold effects.
702 *Biochem J* 2003, **370**(Pt 3): 751-762.
- 703
704 9. Munkácsy E, Rea SL. The paradox of mitochondrial dysfunction and extended longevity. *Exp Gerontol*
705 2014, **56**(0): 221-233.
- 706
707 10. Arnould T, Michel S, Renard P. Mitochondria Retrograde Signaling and the UPR(mt): Where Are We in
708 Mammals? *Int J Mol Sci* 2015, **16**(8): 18224-18251.
- 709
710 11. Nargund AM, Pellegrino MW, Fiorese CJ, Baker BM, Haynes CM. Mitochondrial import efficiency of
711 ATFS-1 regulates mitochondrial UPR activation. *Science* 2012, **337**(6094): 587-590.
- 712
713 12. Biswas G, Adebajo OA, Freedman BD, Anandatheerthavarada HK, Vijayasarathy C, Zaidi M, *et al.*
714 Retrograde Ca²⁺ signaling in C2C12 skeletal myocytes in response to mitochondrial genetic and
715 metabolic stress: a novel mode of inter-organelle crosstalk. *The EMBO Journal* 1999, **18**(3): 522-533.

- 716
717 13. Munkacsy E, Khan MH, Lane RK, Borrer MB, Park JH, Bokov AF, *et al.* DLK-1, SEK-3 and PMK-3 Are
718 Required for the Life Extension Induced by Mitochondrial Bioenergetic Disruption in *C. elegans*. *PLoS*
719 *Genet* 2016, **12**(7): e1006133.
- 720
721 14. Heo JM, Livnat-Levanon N, Taylor EB, Jones KT, Dephore N, Ring J, *et al.* A stress-responsive system for
722 mitochondrial protein degradation. *Mol Cell* 2010, **40**(3): 465-480.
- 723
724 15. Quiros PM, Mottis A, Auwerx J. Mitonuclear communication in homeostasis and stress. *Nat Rev Mol Cell*
725 *Biol* 2016.
- 726
727 16. Schiavi A, Maglioni S, Palikaras K, Shaik A, Strappazon F, Brinkmann V, *et al.* Iron-Starvation-Induced
728 Mitophagy Mediates Lifespan Extension upon Mitochondrial Stress in *C. elegans*. *Curr Biol* 2015, **25**(14):
729 1810-1822.
- 730
731 17. Jiang P, Jin X, Peng Y, Wang M, Liu H, Liu X, *et al.* The exome sequencing identified the mutation in
732 YARS2 encoding the mitochondrial tyrosyl-tRNA synthetase as a nuclear modifier for the phenotypic
733 manifestation of Leber's hereditary optic neuropathy-associated mitochondrial DNA mutation. *Hum Mol*
734 *Genet* 2016, **25**(3): 584-596.
- 735
736 18. Huyen Y, Jeffrey PD, Derry WB, Rothman JH, Pavletich NP, Stavridi ES, *et al.* Structural Differences in the
737 DNA Binding Domains of Human p53 and Its *C. elegans* Ortholog Cep-1. *Structure* 2004, **12**(7): 1237-
738 1243.
- 739
740 19. Ventura N, Rea SL, Schiavi A, Torgovnick A, Testi R, Johnson TE. p53/CEP-1 increases or decreases
741 lifespan, depending on level of mitochondrial bioenergetic stress. *Aging Cell* 2009, **8**(4): 380-393.
- 742
743 20. Schiavi A, Torgovnick A, Kell A, Megalou E, Castelein N, Guccini I, *et al.* Autophagy induction extends
744 lifespan and reduces lipid content in response to frataxin silencing in *C. elegans*. *Experimental*
745 *Gerontology* 2013, **48**(2): 191-201.
- 746
747 21. Lovejoy CA, Cortez D. Common mechanisms of PIKK regulation. *DNA Repair (Amst)* 2009, **8**(9): 1004-
748 1008.
- 749
750 22. Matsuoka S, Ballif BA, Smogorzewska A, McDonald ER, III, Hurov KE, Luo J, *et al.* ATM and ATR Substrate
751 Analysis Reveals Extensive Protein Networks Responsive to DNA Damage. *Science* 2007, **316**(5828):
752 1160-1166.
- 753
754 23. Marechal A, Zou L. DNA damage sensing by the ATM and ATR kinases. *Cold Spring Harb Perspect Biol*
755 2013, **5**(9).
- 756
757 24. Vousden KH, Lane DP. p53 in health and disease. *Nat Rev Mol Cell Biol* 2007, **8**(4): 275-283.
- 758

- 759 25. Yang DQ, Kastan MB. Participation of ATM in insulin signalling through phosphorylation of eIF-4E-
760 binding protein 1. *Nat Cell Biol* 2000, **2**(12): 893-898.
- 761
- 762 26. Schneider JG, Finck BN, Ren J, Standley KN, Takagi M, Maclean KH, *et al.* ATM-dependent suppression of
763 stress signaling reduces vascular disease in metabolic syndrome. *Cell Metab* 2006, **4**(5): 377-389.
- 764
- 765 27. Cosentino C, Grieco D, Costanzo V. ATM activates the pentose phosphate pathway promoting anti-
766 oxidant defence and DNA repair. *EMBO J* 2011, **30**(3): 546-555.
- 767
- 768 28. Schroeder EA, Raimundo N, Shadel GS. Epigenetic silencing mediates mitochondria stress-induced
769 longevity. *Cell Metabolism* 2013, **17**(6): 954-964.
- 770
- 771 29. Fang EF, Bohr VA. NAD⁺: The convergence of DNA repair and mitophagy. *Autophagy* 2017, **13**(2): 442-
772 443.
- 773
- 774 30. Chiolo I, Minoda A, Colmenares SU, Polyzos A, Costes SV, Karpen GH. Double-strand breaks in
775 heterochromatin move outside of a dynamic HP1a domain to complete recombinational repair. *Cell*
776 2011, **144**(5): 732-744.
- 777
- 778 31. Gupta A, Sharma S, Reichenbach P, Marjavaara L, Nilsson AK, Lingner J, *et al.* Telomere length
779 homeostasis responds to changes in intracellular dNTP pools. *Genetics* 2013, **193**(4): 1095-1105.
- 780
- 781 32. Kumar A, Mazzanti M, Mistrik M, Kosar M, Beznoussenko GV, Mironov AA, *et al.* ATR mediates a
782 checkpoint at the nuclear envelope in response to mechanical stress. *Cell* 2014, **158**(3): 633-646.
- 783
- 784 33. Hilton BA, Li Z, Musich PR, Wang H, Cartwright BM, Serrano M, *et al.* ATR Plays a Direct Antiapoptotic
785 Role at Mitochondria, which Is Regulated by Prolyl Isomerase Pin1. *Mol Cell* 2015, **60**(1): 35-46.
- 786
- 787 34. Yi C, Tong J, Lu P, Wang Y, Zhang J, Sun C, *et al.* Formation of a Snf1-Mec1-Atg1 Module on Mitochondria
788 Governs Energy Deprivation-Induced Autophagy by Regulating Mitochondrial Respiration. *Dev Cell* 2017,
789 **41**(1): 59-71 e54.
- 790
- 791 35. Rea SL, Ventura N, Johnson TE. Relationship Between Mitochondrial Electron Transport Chain
792 Dysfunction, Development, and Life Extension in *Caenorhabditis elegans*. *PLoS Biol* 2007, **5**(10): e259.
- 793
- 794 36. Melo JA, Ruvkun G. Inactivation of conserved *C. elegans* genes engages pathogen- and xenobiotic-
795 associated defenses. *Cell* 2012, **149**(2): 452-466.
- 796
- 797 37. Bennett CF, Kwon JJ, Chen C, Russell J, Acosta K, Burnaevskiy N, *et al.* Transaldolase inhibition impairs
798 mitochondrial respiration and induces a starvation-like longevity response in *Caenorhabditis elegans*.
799 *PLoS Genet* 2017, **13**(3): e1006695.

800

- 801 38. Satsuka A, Mehta K, Laimins L. p38MAPK and MK2 pathways are important for the differentiation-
802 dependent human papillomavirus life cycle. *J Virol* 2015, **89**(3): 1919-1924.
- 803
- 804 39. Reinhardt HC, Aslanian AS, Lees JA, Yaffe MB. p53-Deficient Cells Rely on ATM- and ATR-Mediated
805 Checkpoint Signaling through the p38MAPK/MK2 Pathway for Survival after DNA Damage. *Cancer Cell*
806 2007, **11**(2): 175-189.
- 807
- 808 40. Manke IA, Nguyen A, Lim D, Stewart MQ, Elia AE, Yaffe MB. MAPKAP kinase-2 is a cell cycle checkpoint
809 kinase that regulates the G2/M transition and S phase progression in response to UV irradiation. *Mol*
810 *Cell* 2005, **17**(1): 37-48.
- 811
- 812 41. Garcia-Muse T, Boulton SJ. Distinct modes of ATR activation after replication stress and DNA double-
813 strand breaks in *Caenorhabditis elegans*. *Embo J* 2005, **24**(24): 4345-4355.
- 814
- 815 42. Dmitrieva NI, Celeste A, Nussenzweig A, Burg MB. Ku86 preserves chromatin integrity in cells adapted to
816 high NaCl. *Proc Natl Acad Sci U S A* 2005, **102**(30): 10730-10735.
- 817
- 818 43. Desler C, Lykke A, Rasmussen LJ. The effect of mitochondrial dysfunction on cytosolic nucleotide
819 metabolism. *J Nucleic Acids* 2010, **2010**.
- 820
- 821 44. Kuchta RD, Stengel G. Mechanism and evolution of DNA primases. *Biochim Biophys Acta* 2010, **1804**(5):
822 1180-1189.
- 823
- 824 45. Guillian TA, Keen BA, Brissett NC, Doherty AJ. Primase-polymerases are a functionally diverse
825 superfamily of replication and repair enzymes. *Nucleic Acids Res* 2015, **43**(14): 6651-6664.
- 826
- 827 46. Zou L, Elledge SJ. Sensing DNA damage through ATRIP recognition of RPA-ssDNA complexes. *Science*
828 2003, **300**(5625): 1542-1548.
- 829
- 830 47. Tsang WY, Lemire BD. Mitochondrial Genome Content Is Regulated during Nematode Development.
831 *Biochemical and Biophysical Research Communications* 2002, **291**(1): 8-16.
- 832
- 833 48. Derheimer FA, O'Hagan HM, Krueger HM, Hanasoge S, Paulsen MT, Ljungman M. RPA and ATR link
834 transcriptional stress to p53
835 10.1073/pnas.0705317104. *PNAS* 2007: 0705317104.
- 836
- 837 49. Hamperl S, Cimprich KA. The contribution of co-transcriptional RNA:DNA hybrid structures to DNA
838 damage and genome instability. *DNA Repair (Amst)* 2014, **19**: 84-94.
- 839
- 840 50. Zhang ZZ, Pannunzio NR, Hsieh CL, Yu K, Lieber MR. Complexities due to single-stranded RNA during
841 antibody detection of genomic rna:dna hybrids. *BMC Res Notes* 2015, **8**: 127.
- 842

- 843 51. Sollier J, Cimprich KA. Breaking bad: R-loops and genome integrity. *Trends Cell Biol* 2015, **25**(9): 514-522.
844
- 845 52. Proudfoot NJ, Furger A, Dye MJ. Integrating mRNA processing with transcription. *Cell* 2002, **108**(4): 501-
846 512.
- 847
- 848 53. Heintz C, Doktor TK, Lanjuin A, Escoubas C, Zhang Y, Weir HJ, *et al.* Splicing factor 1 modulates dietary
849 restriction and TORC1 pathway longevity in *C. elegans*. *Nature* 2017, **541**(7635): 102-106.
- 850
- 851 54. Kuroyanagi H, Kobayashi T, Mitani S, Hagiwara M. Transgenic alternative-splicing reporters reveal tissue-
852 specific expression profiles and regulation mechanisms in vivo. *Nat Methods* 2006, **3**(11): 909-915.
- 853
- 854 55. Kuroyanagi H, Watanabe Y, Suzuki Y, Hagiwara M. Position-dependent and neuron-specific splicing
855 regulation by the CELF family RNA-binding protein UNC-75 in *Caenorhabditis elegans*. *Nucleic Acids Res*
856 2013, **41**(7): 4015-4025.
- 857
- 858 56. Ventura N, Rea SL. *Caenorhabditis elegans* mitochondrial mutants as an investigative tool to study
859 human neurodegenerative diseases associated with mitochondrial dysfunction. *Biotechnology Journal*
860 2007, **2**(5): 584-595.
- 861
- 862 57. Mori C, Takanami T, Higashitani A. Maintenance of mitochondrial DNA by the *Caenorhabditis elegans*
863 ATR checkpoint protein ATL-1. *Genetics* 2008, **180**(1): 681-686.
- 864
- 865 58. Henderson ST, Bonafe M, Johnson TE. *daf-16* protects the nematode *Caenorhabditis elegans* during food
866 deprivation. *J Gerontol A Biol Sci Med Sci* 2006, **61**(5): 444-460.
- 867
- 868 59. Bloss TA, Witze ES, Rothman JH. Suppression of CED-3-independent apoptosis by mitochondrial
869 [β]NAC in *Caenorhabditis elegans*. *Nature* 2003, **424**(6952): 1066-1071.
- 870
- 871 60. Arsenovic PT, Maldonado AT, Colletuori VD, Bloss TA. Depletion of the *C. elegans* NAC engages the
872 unfolded protein response, resulting in increased chaperone expression and apoptosis. *PLoS ONE* 2012,
873 **7**(9): e44038.
- 874
- 875 61. Kim SK, Lund J, Kiraly M, Duke K, Jiang M, Stuart JM, *et al.* A gene expression map for *Caenorhabditis*
876 *elegans*. *Science* 2001, **293**(5537): 2087-2092.
- 877
- 878 62. Houtkooper RH, Mouchiroud L, Ryu D, Moullan N, Katsyuba E, Knott G, *et al.* Mitonuclear protein
879 imbalance as a conserved longevity mechanism. *Nature* 2013, **497**(7450): 451-457.
- 880
- 881 63. West AP, Khoury-Hanold W, Staron M, Tal MC, Pineda CM, Lang SM, *et al.* Mitochondrial DNA stress
882 primes the antiviral innate immune response. *Nature* 2015, **520**(7548): 553-557.
- 883

- 884 64. Lewis SC, Joers P, Willcox S, Griffith JD, Jacobs HT, Hyman BC. A rolling circle replication mechanism
885 produces multimeric lariats of mitochondrial DNA in *Caenorhabditis elegans*. *PLoS Genet* 2015, **11**(2):
886 e1004985.
- 887
888 65. Starokadomskyy P, Gemelli T, Rios JJ, Xing C, Wang RC, Li H, *et al.* DNA polymerase-alpha regulates the
889 activation of type I interferons through cytosolic RNA:DNA synthesis. *Nat Immunol* 2016, **17**(5): 495-504.
- 890
891 66. Milenkovic D, Blaza JN, Larsson NG, Hirst J. The Enigma of the Respiratory Chain Supercomplex. *Cell*
892 *Metab* 2017, **25**(4): 765-776.
- 893
894 67. George R, Beddoe T, Landl K, Lithgow T. The yeast nascent polypeptide-associated complex initiates
895 protein targeting to mitochondria in vivo. *Proc Natl Acad Sci U S A* 1998, **95**(5): 2296-2301.
- 896
897 68. George R, Walsh P, Beddoe T, Lithgow T. The nascent polypeptide-associated complex (NAC) promotes
898 interaction of ribosomes with the mitochondrial surface in vivo. *FEBS Lett* 2002, **516**(1-3): 213-216.
- 899
900 69. Yogev O, Karniely S, Pines O. Translation-coupled translocation of yeast fumarase into mitochondria in
901 vivo. *J Biol Chem* 2007, **282**(40): 29222-29229.
- 902
903 70. Yang K-S, Kim H-S, Jin U-H, Lee S, Park J-A, Lim Y, *et al.* Silencing of NbBTF3 results in developmental
904 defects and disturbed gene expression in chloroplasts and mitochondria of higher plants. *Planta* 2007,
905 **225**(6): 1459-1469.
- 906
907 71. del Alamo M, Hogan DJ, Pechmann S, Albanese V, Brown PO, Frydman J. Defining the specificity of
908 cotranslationally acting chaperones by systematic analysis of mRNAs associated with ribosome-nascent
909 chain complexes. *PLoS Biology* 2011, **9**(7): e1001100.
- 910
911 72. Amanchy R, Periaswamy B, Mathivanan S, Reddy R, Tattikota SG, Pandey A. A curated compendium of
912 phosphorylation motifs. *Nat Biotechnol* 2007, **25**(3): 285-286.
- 913
914 73. Johnson SC, Yanos ME, Kayser EB, Quintana A, Sangesland M, Castanza A, *et al.* mTOR inhibition
915 alleviates mitochondrial disease in a mouse model of Leigh syndrome. *Science* 2013, **342**(6165): 1524-
916 1528.
- 917
918 74. Zid BM, Rogers AN, Katewa SD, Vargas MA, Kolipinski MC, Lu TA, *et al.* 4E-BP extends lifespan upon
919 dietary restriction by enhancing mitochondrial activity in *Drosophila*. *Cell* 2009, **139**(1): 149-160.
- 920
921 75. Bonawitz ND, Chatenay-Lapointe M, Pan Y, Shadel GS. Reduced TOR Signaling Extends Chronological Life
922 Span via Increased Respiration and Upregulation of Mitochondrial Gene Expression. *Cell Metab* 2007,
923 **5**(4): 265-277.
- 924
925 76. Garelick MG, Mackay VL, Yanagida A, Academia EC, Schreiber KH, Ladiges WC, *et al.* Chronic rapamycin
926 treatment or lack of S6K1 does not reduce ribosome activity in vivo. *Cell Cycle* 2013, **12**(15): 2493-2504.

- 927
928 77. Wood WB (ed). *The Nematode Caenorhabditis elegans*. Cold Spring Harbor Laboratory: New York, 1988.
- 929
930 78. Timmons L, Fire A. Specific interference by ingested dsRNA. *Nature* 1998, **395**(6705): 854.
- 931
932 79. Hoogewijs D, Houthoofd K, Matthijssens F, Vandesompele J, Vanfleteren JR. Selection and validation of a
933 set of reliable reference genes for quantitative sod gene expression analysis in *C. elegans*. *BMC Mol Biol*
934 2008, **9**: 9.
- 935
936 80. Sugimoto T, Mori C, Takanami T, Sasagawa Y, Saito R, Ichiishi E, *et al.* *Caenorhabditis elegans*
937 *par2.1/mtssb-1* is essential for mitochondrial DNA replication and its defect causes comprehensive
938 transcriptional alterations including a hypoxia response. *Experimental Cell Research* 2008, **314**(1): 103-
939 114.
- 940
941 81. Rooney JP, Ryde IT, Sanders LH, Howlett EH, Colton MD, Germ KE, *et al.* PCR based determination of
942 mitochondrial DNA copy number in multiple species. *Methods Mol Biol* 2015, **1241**: 23-38.
- 943
944 82. Kuroyanagi H, Ohno G, Sakane H, Maruoka H, Hagiwara M. Visualization and genetic analysis of
945 alternative splicing regulation in vivo using fluorescence reporters in transgenic *Caenorhabditis elegans*.
946 *Nat Protoc* 2010, **5**(9): 1495-1517.
- 947
948 83. Luz AL, Rooney JP, Kubik LL, Gonzalez CP, Song DH, Meyer JN. Mitochondrial Morphology and
949 Fundamental Parameters of the Mitochondrial Respiratory Chain Are Altered in *Caenorhabditis elegans*
950 Strains Deficient in Mitochondrial Dynamics and Homeostasis Processes. *PLoS One* 2015, **10**(6):
951 e0130940.
- 952
953 84. Steffen KK, MacKay VL, Kerr EO, Tsuchiya M, Hu D, Fox LA, *et al.* Yeast life span extension by depletion of
954 60s ribosomal subunits is mediated by Gcn4. *Cell* 2008, **133**(2): 292-302.
- 955
956 85. Torgovnick A, Schiavi A, Shaik A, Kassahun H, Maglioni S, Rea SL, *et al.* BRCA1 and BARD1 mediate
957 apoptotic resistance but not longevity upon mitochondrial stress in *Caenorhabditis elegans*. *EMBO Rep*
958 2018, **19**(12).

959
960

961 SUPPLEMENTAL MATERIAL

962 SUPPLEMENTAL FIGURES

963 **Figure S1.** Loss of ATL-1 desensitizes worms to mitochondrial respiratory chain stress induced by ethidium
964 bromide.

965 **Figure S2.** DNA mutation detection in *C. elegans* using β -Gal frame-shift- and TUNEL assays.

966 **Figure S3.** Nucleotide biosynthesis in *C. elegans* highlighting the role of the mitochondrial ETC.

967 **Figure S4.** mRNA splicing remains unaltered in worms experiencing ETC disruption, both in the
968 absence or presence of *atf-1* knockdown.

969 **Figure S5.** *atf-1* knockdown does not alter retrograde response pathways normally induced by
970 mitochondrial ETC stress.

971

972 **SUPPLEMENTAL TABLES**

973 **Table S1.** Summary of descriptive statistics for final-round DDR test RNAi screen hits. (Related to **Fig.**
974 **3**).

975 **Table S2.** Mean Ranks of final-round DDR RNAi hits used for Kruskal-Wallis test. (Related to **Fig. 3**).

976 **Table S3.** Post-hoc tests for each final-round DDR RNAi hit versus vector. (Related to **Fig. 3**).

977 **Table S4.** List of *C. elegans* strains employed in current study.

978 **Table S5.** qPCR primer list.

979

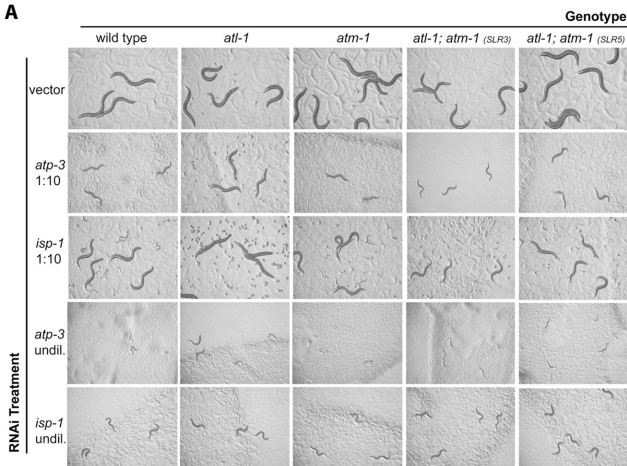
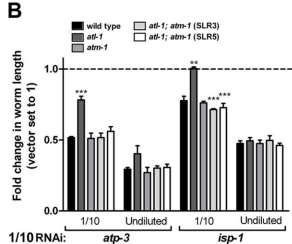
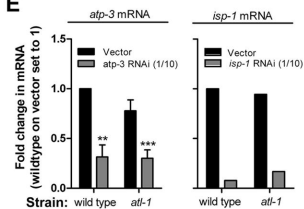
980 **OTHER SUPPLEMENTAL FILES**

981 **File S1.** Supplemental Methods & Supplemental Figure Legends

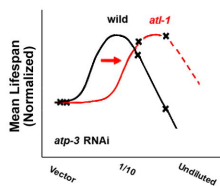
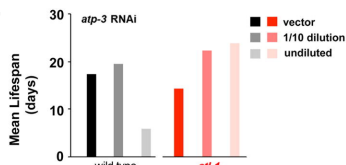
982 **File S2.** Mean difference ratios of all hits from DNA Damage Response (DDR) screen. (Related to **Fig.**
983 **3**)

984 **File S3.** Significance testing for differences in HXK2::GFP fluorescence. (related to **Fig. 7C**)

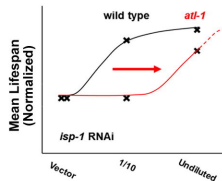
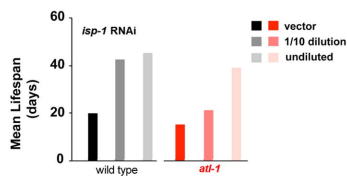
985

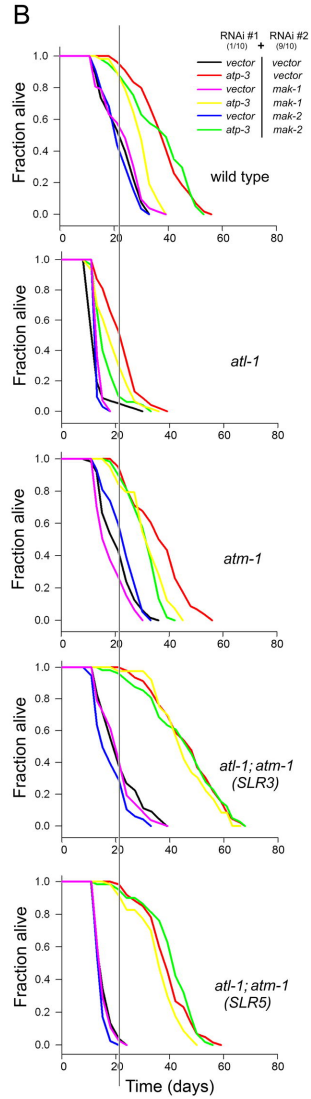
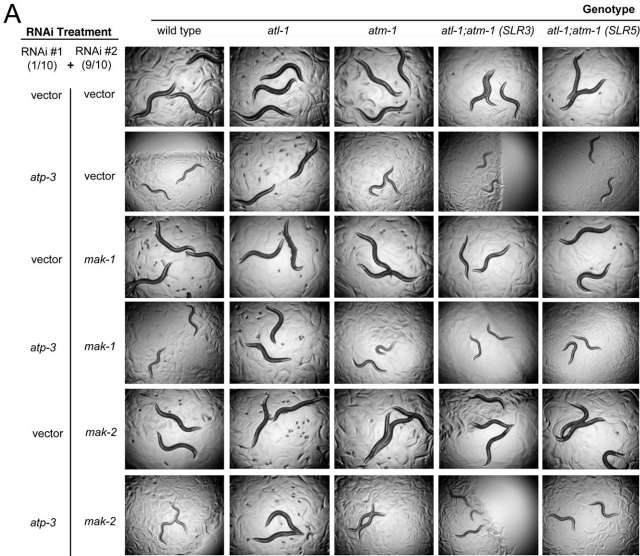
A**B****E****C**

Genotype (Strain)	Condition	Mean Lifespan (days)	n	Log Rank Comparison (vs. within-strain control)
wild type (SLR4)	Control	18.9	70	-
	1/10 <i>atp-3</i>	20.7	58	0.007
	Undiluted <i>atp-3</i>	6.9	62	2.56E-25
<i>atf-1</i> (SLR1)	Control	15.4	70	-
	1/10 <i>atp-3</i>	23.4	63	4.33E-10
	Undiluted <i>atp-3</i>	24.9	67	2.09E-11
<i>atm-1</i> (SLR2)	Control	20.8	70	-
	1/10 <i>atp-3</i>	14.2	43	0.0008
	Undiluted <i>atp-3</i>	5.8	53	1.00E-29
<i>atf-1; atm-1</i> (SLR3)	Control	20.5	69	-
	1/10 <i>atp-3</i>	28.3	67	7.31E-08
	Undiluted <i>atp-3</i>	7.0	63	6.24E-24
<i>atf-1; atm-1</i> (SLR5)	Control	16.1	65	-
	1/10 <i>atp-3</i>	30.8	30	8.94E-10
	Undiluted <i>atp-3</i>	9.1	22	0.017

**D**

Genotype (Strain)	Condition	Mean Lifespan (days)	n	Log Rank Comparison (vs. within-strain control)
wild type (SLR4)	Control	21.9	70	-
	1/10 <i>isp-1</i>	43.1	72	1.30E-16
	Undiluted <i>isp-1</i>	47.0	69	6.17E-12
<i>atf-1</i> (SLR1)	Control	18.4	70	-
	1/10 <i>isp-1</i>	22.9	70	0.547
	Undiluted <i>isp-1</i>	39.6	70	4.89E-07
<i>atm-1</i> (SLR2)	Control	20.2	70	-
	1/10 <i>isp-1</i>	44.0	70	4.76E-15
	Undiluted <i>isp-1</i>	48.1	72	5.24E-12
<i>atf-1; atm-1</i> (SLR3)	Control	22.7	72	-
	1/10 <i>isp-1</i>	51.2	69	9.87E-23
	Undiluted <i>isp-1</i>	58.9	74	2.43E-24
<i>atf-1; atm-1</i> (SLR5)	Control	17.4	69	-
	1/10 <i>isp-1</i>	38.1	44	1.17E-11
	Undiluted <i>isp-1</i>	51.2	56	1.60E-16

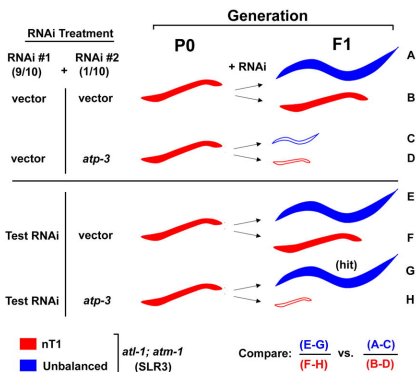




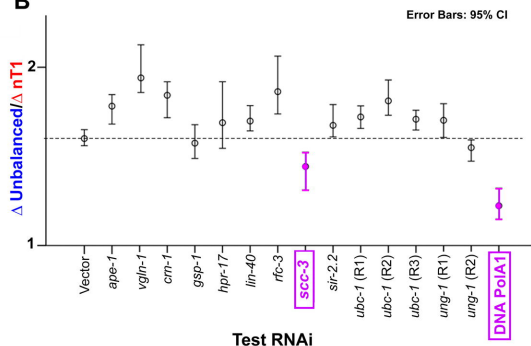
C

Genotype (Strain)*	ID	Conditions RNAi #1 (1/10)	Conditions RNAi #2 (9/10)	Mean Lifespan (days)	n	Log Rank (vs. A1)	Log Rank (vs. A2)	Log Rank (A2 vs. A1; B2 vs. B1; C2 vs. C1)
Wild type (SLR4)	A1	vector	vector	22.6	60	-	-	-
	A2	<i>atp-3</i>	vector	38.4	59	-	-	1.93E-15
	B1	vector	<i>mak-1</i>	23.5	60	0.43	-	-
	B2	<i>atp-3</i>	<i>mak-1</i>	39.2	60	-	1.21E-7	0.00013
	C1	vector	<i>mak-2</i>	22.1	60	0.48	-	-
	C2	<i>atp-3</i>	<i>mak-2</i>	37.4	60	-	0.97	7.95E-13
<i>atf-1</i> (SLR1)	A1	vector	vector	13.2	60	-	-	-
	A2	<i>atp-3</i>	vector	22.6	60	-	-	4.17E-09
	B1	vector	<i>mak-1</i>	14	60	0.04	-	-
	B2	<i>atp-3</i>	<i>mak-1</i>	19.3	60	-	0.04	0.008
	C1	vector	<i>mak-2</i>	13.3	60	0.19	-	-
	C2	<i>atp-3</i>	<i>mak-2</i>	17	60	-	0.0003	0.0015
<i>atm-1</i> (SLR2)	A1	vector	vector	21.0	64	-	-	-
	A2	<i>atp-3</i>	vector	36.9	60	-	-	1.83E-14
	B1	vector	<i>mak-1</i>	18.5	60	0.06	-	-
	B2	<i>atp-3</i>	<i>mak-1</i>	32.5	60	-	0.003	1.32E-14
	C1	vector	<i>mak-2</i>	23.3	60	0.19	-	-
	C2	<i>atp-3</i>	<i>mak-2</i>	31.5	60	-	9.73E-5	2.30E-09
<i>atf-1; atm-1</i> (SLR3)	A1	vector	vector	21.8	60	-	-	-
	A2	<i>atp-3</i>	vector	47.1	60	-	-	3.70E-16
	B1	vector	<i>mak-1</i>	21.3	60	0.88	-	-
	B2	<i>atp-3</i>	<i>mak-1</i>	45.8	60	-	0.43	8.40E-16
	C1	vector	<i>mak-2</i>	18.3	60	0.03	-	-
	C2	<i>atp-3</i>	<i>mak-2</i>	45.8	61	-	0.96	2.84E-18
<i>atf-1; atm-1</i> (SLR5)	A1	vector	vector	15.8	60	-	-	-
	A2	<i>atp-3</i>	vector	39.6	60	-	-	3.89E-23
	B1	vector	<i>mak-1</i>	15.6	60	0.74	-	-
	B2	<i>atp-3</i>	<i>mak-1</i>	36.3	60	-	0.04	5.92E-20
	C1	vector	<i>mak-2</i>	14.7	70	0.18	-	-
	C2	<i>atp-3</i>	<i>mak-2</i>	41.2	60	-	0.40	1.33E-20

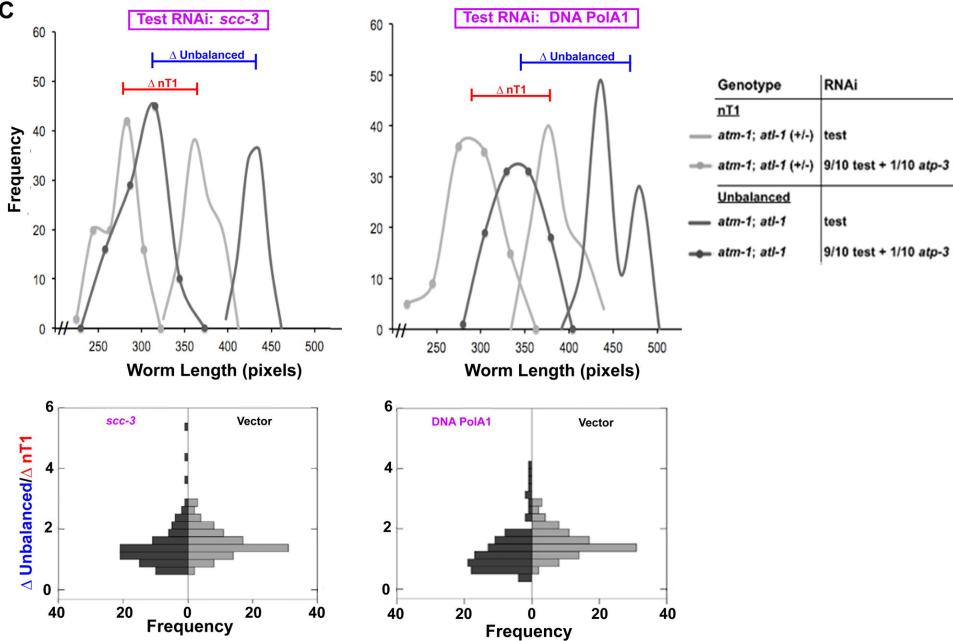
A Screening Method



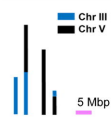
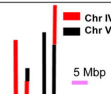
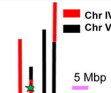
B



C



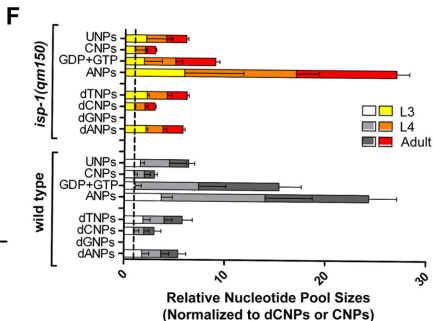
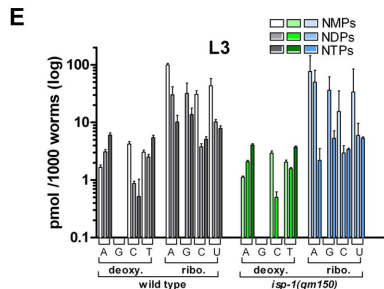
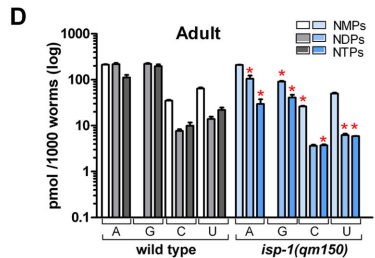
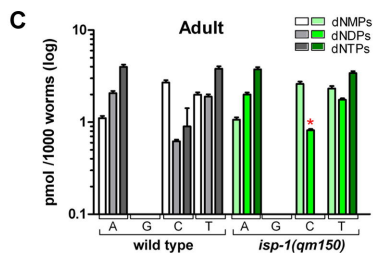
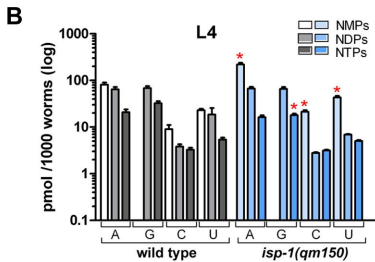
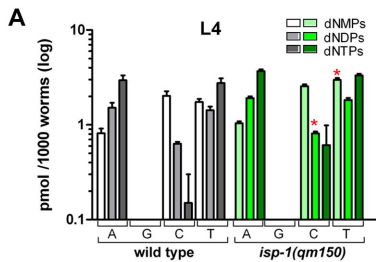
A

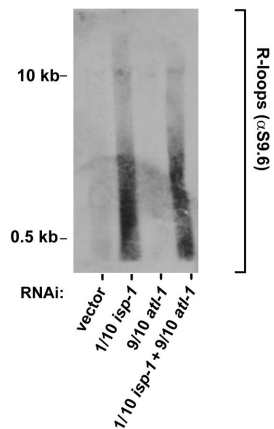
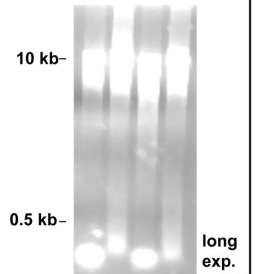
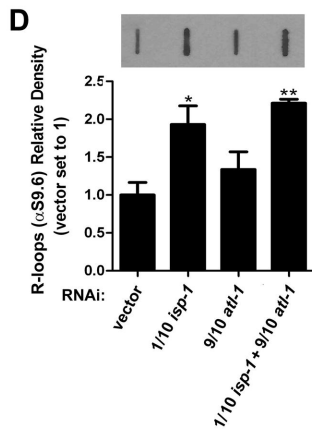
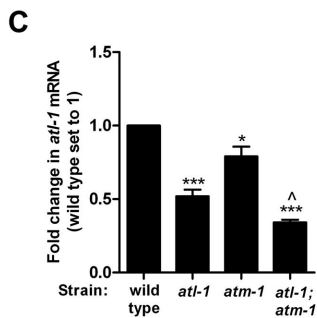
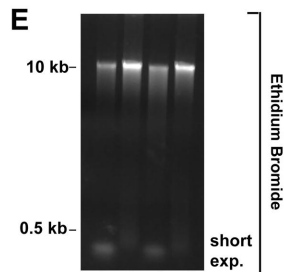
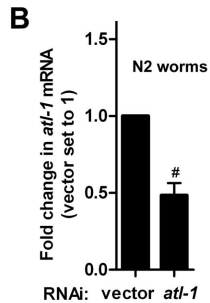
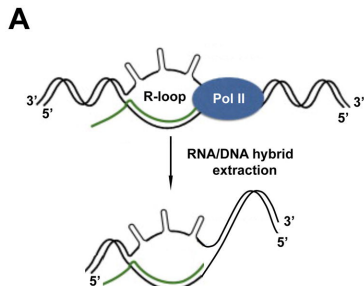
Genotype	Genome Coverage *	<i>atp-3</i> : Vector RNAi Ratio	F1 Animals Scored	Mutants Detected	Mutant Frequency (%)	Fisher's Exact Test P-value
<i>dpy-18(e364)/eT1 III</i> ; <i>unc-46(e177)/eT1 V</i> .		Vector	152	0	0	--
		1:200	173	0	0	1
		1:100	187	0	0	1
		1:50	187	0	0	1
		1:20	177	0	0	1
		1:10	187	1	0.5	1
nT1 (IV;V)		Vector	1292	4	0.31	--
		1:20	858	5	0.58	0.497
nT1 (IV;V) (<i>qls50</i>)		Vector	671	1	0.15	--
		1:20	674	0	0.00	0.499

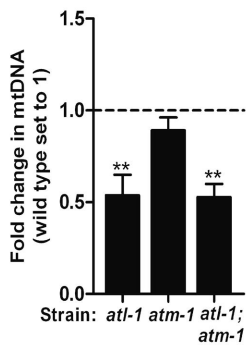
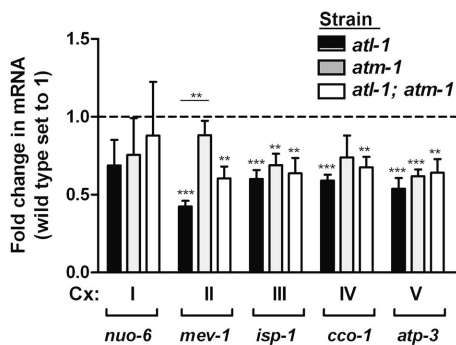
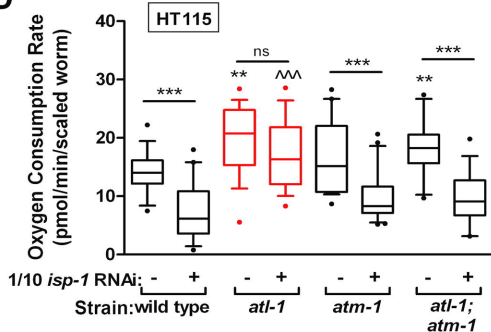
*Chromosomes drawn to scale. Green star in schematic indicates the presence of GFP marker.

B

Genotype	RNAi (Dilution)	Plates Scored	Plate Reversion Frequency (%)	Fisher's Exact Test P-value
<i>unc-58</i> (<i>e665</i>)	Vector	63	0	--
	<i>atp-3</i> (1:20)	63	0	1
	<i>rpa-1</i> (1:10)	64	23.4	<0.001
<i>unc-93</i> (<i>e1500</i>)	Vector	48	27.1	--
	<i>atp-3</i> (1:20)	88	22.7	0.687
	<i>rpa-1</i> (1:10)	36	63.9	0.001





A**B****D****C**

HXK-2::GFP Reporter

RNAi treatment (vector balance)

